DESIGN AND MANUFACTURING OF A SINGLE LANGMUIR PROBE FOR PLASMA MEASUREMENTS IN HALL EFFECT THRUSTER EXPERIMENTS

A THESIS SUBMITTED TO
THE GRADUATE SCHOOL OF NATURAL AND APPLIED SCIENCES
OF
MIDDLE EAST TECHNICAL UNIVERSITY

BY

ÖZGE YAZICIOĞLU

IN PARTIAL FULFILLMENT OF THE REQUIREMENTS
FOR
THE DEGREE OF MASTER OF SCIENCE
IN
AEROSPACE ENGINEERING

SEPTEMBER 2014

Approval of the thesis:

DESIGN AND MANUFACTURING OF A SINGLE LANGMUIR PROBE FOR PLASMA MEASUREMENTS IN HALL EFFECT THRUSTER EXPERIMENTS

submitted by **ÖZGE YAZICIOĞLU** in partial fulfillment of the requirements for the degree of **Master of Science in Aerospace Engineering Department, Middle East Technical University** by,

Prof. Dr. Canan Özgen _____
Dean, Graduate School of **Natural and Applied Sciences**

Prof. Dr. Ozan Tekinalp _____
Head of Department, **Aerospace Engineering**

Prof. Dr. Nafiz Alemdaroğlu _____
Supervisor, **Aerospace Engineering Department, METU**

Dr. Demet Uluşen _____
Co-supervisor, **TÜBİTAK Space Technologies Research Institute**

Examining Committee Members

Prof. Dr. Altan Kayran _____
Aerospace Engineering Dept., METU

Prof. Dr. Nafiz Alemdaroğlu _____
Aerospace Engineering Dept., METU

Dr. Demet Uluşen _____
Tubitak Space Technologies Research Institute

Assoc. Prof. Dr. D. Funda Kurtuluş _____
Aerospace Engineering Dept., METU

Assoc. Prof. Dr. İsmail Rafatov _____
Physics Dept., METU

Date: September 4, 2014

I hereby declare that all information in this document has been obtained and presented in accordance with academic rules and ethical conduct. I also declare that, as required by these rules and conduct, I have fully cited and referenced all material and results that are not original to this work.

Name, Last Name: ÖZGE YAZICIOĞLU

Signature:

ABSTRACT

DESIGN AND MANUFACTURING OF A SINGLE LANGMUIR PROBE FOR PLASMA MEASUREMENTS IN HALL EFFECT THRUSTER EXPERIMENTS

Yazıcıoğlu, Özge
M.S., Department of Aerospace Engineering
Supervisor : Prof. Dr. Nafiz Alemdaroğlu
Co-Supervisor: Dr. Demet Uluşen

September 2014, 81 pages

Electric propulsion is a technology which has been tested on ground and in space since 1960s. The goal of electric propulsion systems is to achieve thrust with high exhaust velocities using electricity. To date, more than 200 electric thrusters have been flown and operated successfully onboard communication satellites and deep-space scientific missions for years with zero failure rate, making the technology more attractive in recent years. Thrust, specific impulse, total efficiency and plume divergence are some figures of merit for the performance of the thruster. Different probes are used in plasma measurements to evaluate and test the performance of the Hall Effect Thrusters. In this study, a Single Langmuir probe design is given for plasma measurements in low pressure. The basic working principle of Single Langmuir probe along with the criteria and measurement methodology applied in the design of the probe is also described. In addition, the technique that is used in the analysis of the current-voltage characteristics to determine the local plasma potential, electron number density and temperature is discussed in detail. Then, the designed probe was produced and used for plasma measurements in low pressure vacuum chamber. The results of measurements and the comparisons with that of Standard ALP System Langmuir Probe are presented in detail.

Keywords: Hall Effect Thruster, Single Langmuir Probe Manufacturing, Plasma Diagnostic.

ÖZ

HALL ETKİLİ BİR İTKİ MOTORUNUN PLAZMA ÖLÇÜMLERİNDE KULLANILMAK ÜZERE TEKLİ LANGMUIR PROBE TASARIMI VE ÜRETİMİ

Yazıcıoğlu, Özge

Yüksek Lisans, Havacılık ve Uzay Mühendisliği Bölümü
Tez Yöneticisi : Prof. Dr. Nafiz Alemdaroğlu
Ortak Tez Yöneticisi: Dr. Demet Uluşen

Eylül 2014, 81 sayfa

Elektrikli İtki sistemleri 1960'lardan beri yerde ve uzayda test edilen bir teknolojidir. Elektrikli itki sistemlerinin amacı elektrik kullanılarak yüksek egzoz hızları ile itki elde etmektir. Bugüne kadar 200'den fazla elektrikli itki sistemi iletişim uyduları ve derin-uzay bilimsel görevlerinde başarılı bir şekilde kullanılarak son yıllarda daha cazip hale gelmiştir. İtki, özgül itki, toplam verimlilik ve kuyruk gazı dağılımı iticinin performansını ölçmek için bazı başarım ölçütleridir. Hall Etkili İticinin performansını değerlendirmek için yapılan plazma ölçümlerinde farklı problar kullanılmaktadır. Bu çalışmada, düşük basınç plazma ölçümleri için tekli Langmuir prob tasarımı yapılmıştır. Probun tasarımında kullanılan tasarım kriterleri yanında probun basit çalışma prensibi ve ölçüm metodolojisi de tanımlanmıştır. Akım-voltaj eğrisi analiz tekniği kullanılarak bölgesel plazma potansiyeli, elektron sayı yoğunluğu ve sıcaklık değerleri tartışılmıştır. Daha sonra ise tasarlanan probun üretim detayları verilmiştir. Prob düşük basınçlı vakum odasında kullanılarak, ölçüm sonuçları standart ALP Sistem Probun ölçüm değerleri ile karşılaştırılmıştır.

Anahtar Kelimeler: Hall Etkili İtki Sistemi, Tekli Langmuir Probe Üretimi, Plazma Tanısı.

…To my family

ACKNOWLEDGEMENTS

This work would not have been possible without the support of many people. First of all, I would like to thank my supervisor Prof. Dr. Nafiz Alemdaroğlu and co-supervisor Dr. Demet Uluşen for their guidance and supports throughout the research.

Also, I appreciate to Prof. Dr. Sinan Bilikmen and Plasma Physics Laboratory in METU for usage of their experimental devices, RF Discharge plasma chamber and pump system, plasma Power System, ALP Probe System. Also, I would like to thank Mrs. Doğan Mansuroğlu for his help in Plasma Physics Laboratory and Dr. Ümmügül Erözbek-Güngör for her kind assistance and help during my plasma measurements.

I would also like to thank Prof. Dr. Raşit Turan and his assistant Mr. Mete Günöven for usage of their experimental device, Source Meter and Mr. Engin Kıran for technical support about the probe circuit.

Also, I would like to thank TUBITAK Space Technologies Research Institute for supplying probe materials and its valuable workers, Mr. İsmail Sedat Gülle and Mrs. Banu Çiçek Aydın, for their contribution throughout the process.

I would like to express my deepest thanks to my parents Naciye and Mesut Tabak, my sister Yasemin and my brother Can for their love and support. Also, to my nephew, Mert; thanks for making me smile.

Finally, my special thank go to my husband; Mustafa Yazıcıoğlu, for his confidence, supports and love. He also gave me the strength to finish this work.

TABLE OF CONTENTS

LIST OF TABLES

TABLES

LIST OF FIGURES

FIGURES

CHAPTER 1

INTRODUCTION

1.1 Electric Propulsion

Electric propulsion is a type of spacecraft technology which has been tested on the ground and in space since the 1960s. To date, more than 200 electric thrusters have been flown and operated successfully onboard communication satellites and deep-space scientific missions for years with zero failure rate, making the technology more attractive in recent years [1].

The goal of electric propulsion systems is to achieve thrust with high exhaust velocities using electricity. Achievement of this goal makes the Electric Propulsion (EP) a cost effective solution for many space applications compared to other conventional propulsion methods, such as chemical propulsion. Because providing higher specific impulse (Isp) (which is defined as the propellant exhaust velocity divided by the gravitational acceleration constant g) reduces the amount of propellant required for a specific mission. Less propellant allows for less launch mass of a spacecraft and in return reduces the cost to send the spacecraft to the Earth orbit or to a deep-space target [1,2].

Electric propulsion is different from the chemical propulsion in the method of providing energy necessary to create the thrust. Chemical propulsion systems supply the required energy by breaking the chemical bonds of a propellant, however, in electric propulsion systems; the source of energy is the solar panels, batteries or nuclear power onboard spacecraft. Because the chemical bonds have a restricted energy, the attainable exhaust velocity or specific impulse from the propellant is also limited. For electric propulsion systems, however, there is no such natural limitation as the energy source is separated from the propellant and becomes a power supply which is only limited by the available technology [3]. Therefore, while the exhaust velocity can rise nearly up to 4 km/s in chemical propulsion, the exhaust velocity of

electric thrusters can approach 100 km/s with heavy propellants such as Xenon gas [1].

1.2. Motivation and Objectives

As mentioned in the previous section, Electric Propulsion technology has many advantages for certain space applications. Its main advantage is achieving a thrust with high exhaust velocity and thus reducing the propellant mass required for a specific space task. It is because of this advantage, Electric Propulsion studies date back to 1960s across the world. However, in Turkey, this technology is a new research area and in order to establish the first R&D laboratory in the field of electric propulsion systems, in 2010, TUBITAK-Space Technologies Research Institute (TUBITAK UZAY) started a project called "Hall Effect Thruster Development Project (HALE)" by the financial support from the Turkish Ministry of Development. In addition to this project, a research study ("Design, Production and Test of an Electric Propulsion System to be used in Satellite Systems") was also initiated by Prof. Dr. Nafiz ALEMDAROĞLU at the Department of Aerospace Engineering at Middle East Technical University. The main objective of this study was to produce a Hall Effect Thruster prototype and this thesis was part of it being funded by TUBITAK (with a project code of 109M402). In the scope of both TUBITAK UZAY and METU projects, diagnostics instruments are also aimed to be developed for the measurements of certain plasma parameters, which are needed for the evaluation of the thruster's performance. Therefore, the objective of this thesis is to design and manufacture a single Langmuir probe for plasma measurements in Hall Effect Thruster experiments at TUBITAK UZAY. However, because the thruster and vacuum test facilities are not yet complete in the course of the thesis, the designed and produced single Langmuir Probe is tested in a vacuum chamber available at the METU Plasma Physics Laboratory and the results from these experiments are presented leaving the tests at TUBITAK UZAY as a future follow up work.

1.3. Organization

The main objective of this thesis is to investigate the electric thrusters' diagnostic tools, to design and manufacture a plasma probe and to evaluate the performance of an electric thruster, specifically a Hall Effect Thruster, using this designed probe. Therefore, initially, types of Electric Propulsion and then the fundamentals of Hall Effect Thrusters are introduced in the following chapter. In the literature, various diagnostic techniques are applied in plasma measurements. Different test equipment measures different parameters, such as plasma potential, electron temperature, electron density, and ion energy distribution. In Chapter 3, several plasma instruments utilized in the test of Hall thrusters, including a Langmuir Probe, a Faraday probe, an emissive probe and a retarding potential analyzer, are introduced briefly. As this thesis focuses on a Single Langmuir probe design to be used in Hall thruster's experiments, the basic working principle of Single Langmuir probes along with the criteria and measurement methodology applied in the design of the probe are described in Chapter 4. The techniques that are used in the analysis of the current-voltage characteristics from the probe to determine the local plasma potential, electron number density, and temperature are also discussed in Chapter 4. Then, the materials used in the manufacture of the probe and the end product handmade probe description are presented in detail in Chapter 5. The experimental setup with all equipment in the METU Plasma Physics Laboratory, which are utilized for testing the manufactured probe for plasma measurements in the low pressure vacuum chamber, are introduced in Chapter 6. In order to test the manufactured probe and evaluate the precision of it, a commercial probe (the ALP System Langmuir Probe) is also used in the same vacuum chamber and the results of plasma measurements from both probes are compared in Chapter 7. Finally, in the last chapter (Chapter 8), the main findings of the thesis are summarized and future directions are discussed.

CHAPTER 2

FUNDAMENTALS OF ELECTRIC PROPULSION

Supply of a thrust with very high exhaust velocities by Electric Propulsion (EP) systems offers a very cost effective solution for some space applications when compared to conventional chemical propulsion systems. Availability of higher specific impulse (Isp) reduces the amount of propellant required to perform a specific task and thus also reduces the spacecraft mass. Launching a lighter spacecraft to the Earth orbit or to a deep-space target is more economical and therefore makes this technology very attractive for commercial use.

In a propulsion system, *thrust*, *specific impulse* and *total efficiency*, and their interrelations are important figures of merit as they significantly influence the overall performance of the thruster [1,2]. Thrust is defined as the time rate of change of the momentum,

$$T = \frac{d}{d_t}\left(m_p v_{ex}\right) = \frac{d_{m_p}}{d_t} v_{ex} = \dot{m}_p v_{ex}, \tag{2.1}$$

where T is thrust in N, $\dot{m}_p$ is the propellant mass flow rate in kg/s and v_{ex} is the exhaust velocity in m/s.

Specific impulse (I_{sp}) is a measure of thrust efficiency and is expressed as the ratio of the thrust to the rate of propellant consumption [1],

$$Isp = \frac{T}{\dot{m}_p g}, \tag{2.2}$$

$$Isp = \frac{v_{ex}}{g}. \tag{2.3}$$

The main difference between propulsion systems is the way they provide the energy necessary to create thrust. Chemical propulsion systems, for instance, supply the

required energy from the chemical bonds of the propellant. However, in electric propulsion systems, solar panels, batteries or nuclear power are the source of the energy. Therefore, while the attainable exhaust velocity or specific impulse from the chemical systems is limited to the chemical bond energies, there is no such limitation in the electrical systems. In electric propulsion technology, the energy source is a separate power supply [3]. This advantage permits electric thrusters to create much higher exhaust velocity (up to 100 km/s) when compared to chemical systems (4 km/s). The most efficient propellant for electric thrusters used today is the heavy noble gas, Xenon [1].

To summarize, electric propulsion provides higher specific impulse but lower thrust levels compared to conventional chemical propulsion. Therefore EP systems consume less propellant but longer time to perform the same task when compared to chemical counterparts. In the next section, types of electric propulsion systems are introduced briefly and then compared to chemical systems.

2.1 Electric Thruster Types

There is a wide variety of electric propulsion types. They are commonly classified into three categories based on the underlying physics in their operation; (1) electrothermal, (2) electromagnetic and (3) electrostatic [4]. The fundamental characteristics of the common electric propulsion types are described in the following subsections.

2.1.1 Electrothermal Propulsion:

Electrothermal propulsion relies on the heating of the propellant to increase its exhaust velocity [2]. In these systems, propellant is electrically heated to high temperatures and accelerated through a suitable nozzle [4]. The most common Electrothermal thruster types include Resistojets in which the propellant is heated by passing through a resistively heated element or chamber; and Arcjets in which the propellant is heated with an arc-discharge [1,4]

2.1.2 Electromagnetic Propulsion:

The governing physics of electromagnetic propulsion is the acceleration of the propellant by the force created through interactions of electric and magnetic fields (i.e., Lorentz force). There are different types of electromagnetic propulsion devices, which include Magneto Plasma Dynamic Thrusters (MPDT), Pulsed-Inductive Thrusters (PIT), and Pulsed Plasma Thrusters (PPT) [4].

2.1.3 Electrostatic Propulsion:

Electrostatic propulsion relies on the acceleration of propellant ions through an applied electric field. Main Electrostatic propulsion types include Gridded ion thrusters, Colloid thrusters, Field Emission Electric Propulsion (FEEP), and Hall Effect Thrusters (HET) [4]. As the focus of this thesis is on the HETs, the governing physics of this type of thrusters is presented in detail in the following subsection.

In the following table, comparison of specific impulse created typically by electric and chemical thrusters is illustrated. As seen, in most of the EP systems, the Isp is one order of magnitude greater than the chemical system Isp. This comparison clearly shows that the thrust produced per mass is much higher in the electric propulsion systems.

Table 2.1 Typical performances of electric propulsion types and their comparison to chemical propulsion systems [4]

Thruster Concept	**Specific Impulse [s]**
Chemical Monopropellant	150-225
Chemical Bipropellant	300-450
Electrothermal Propulsion	
Resistojet	300
Arcjet	500-1000
Electromagnetic Propulsion	
Magnetoplasmadynamic Thruster	1000-5000
Pulsed Plasma Thruster	1000-1500
Pulsed Inductive Thruster	2000-8000
Electrostatic Propulsion	
Hall Effect Thruster	1000-8000
Ion Thruster	2000-10000

2.2 Operation of a Hall Effect Thruster

Hall Thrusters were originally discovered independently in the U.S. and former Soviet Union in the mid-1960s. Since then numerous experimental and numerical studies have been performed until the technology has become mature enough for space applications [4]. The first Hall Thruster was developed by the Soviet Union and gained flight heritage on the Meteor spacecraft in 1971 [1].

Although Hall thrusters are relatively simple devices, their operation rely on much more complicated physics than that of the other thrusters in the same class, (e.g., ion thrusters). The efficiency and specific impulse of ion thrusters are typically higher than that of Hall Thrusters, but the thrust to power ratio in Hall Thrusters is greater than the ions thrusters. This means that less power is required to operate HETs. Performance, efficiency, and lifetime of Hall Thrusters are strongly dependent on the

details of the thruster geometry, magnetic field configuration and the materials used in the manufacturing of the thruster components [1].

A Hall Effect Thruster basically consists of three components, which are the cathode, the discharge region, and the magnetic field generator (see Figure 2.1). The discharge region is enclosed by a cylindrical insulating channel, called "discharge channel", usually made up of a ceramic type of material. A radial magnetic field (B) is generated inside the channel by magnetic coils located at the center and around the channel as shown in Figure 2.1.b. Gas, usually Xenon, is injected from the anode at the base and dispersed into the channel. Electrons are supplied from a cathode at the end opposite to the anode. This way an electric field with a dominantly axial component is created along the channel between the anode and cathode. Hall current is created by the electrons spiraling around the thruster axis in the *ExB* direction due to the strong B field. Under the presence of the electric and magnetic field, the neutral gas and electrons collide inside the channel and create *Xe* ions. These ions are then accelerated by the electric field in the axial direction, exhausting out of the channel at high velocities [1,4].

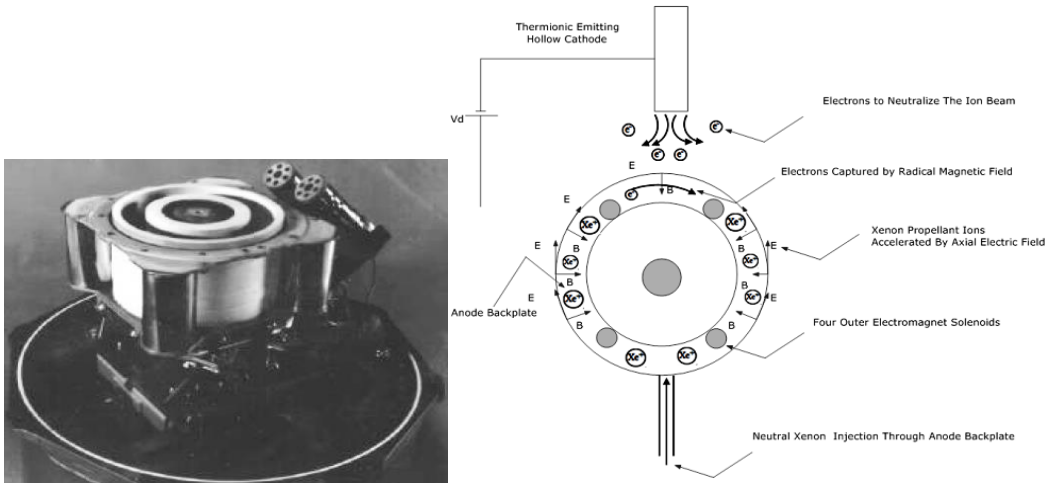

(2.1.a) (2.1.b)

Figure 2.1 Photograph of SPT-100 and schematic of a basic SPT-100 operation [5]

As already mentioned in the previous paragraphs, even though the physical schematic of a Hall thruster operation is simple, the plasma processes in the discharge channel, interrelated field effects, discharge geometry, and cathode coupling effects make the optimum design of high-performance Hall thrusters difficult if not impossible. Therefore, up to date, optimization of Hall thrusters has been largely based on experimental studies and therefore their initial design is usually rely on the empirical scaling laws [4].

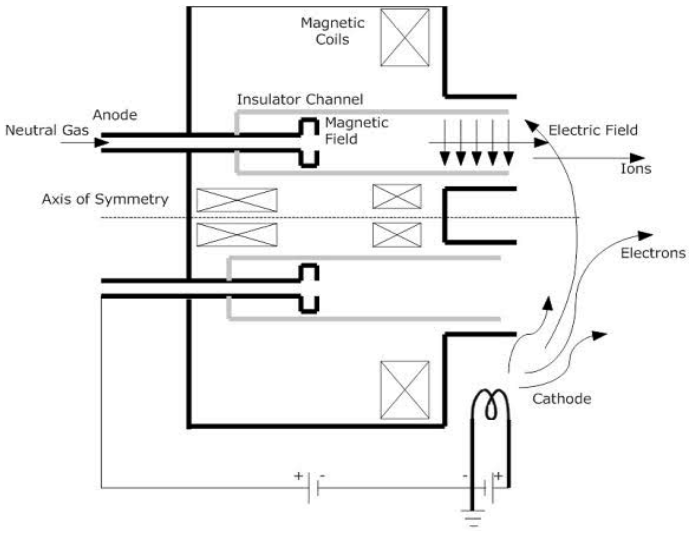

Figure 2.2 Schematic illustration of a Hall thruster showing the radial magnetic field and the accelerating electric field [36]

In Hall Thruster operation, cathode has two functions: The first one is neutralizing the ion beam to prevent the system from charging. The second one is emitting electrons to the anode to sustain the plasma processes [4]. The electrostatic field created between the Hall Thruster anode and cathode accelerates ions, which are only weakly deflected by the imposed radial magnetic field due their heavy mass. The electrons, however, are strongly magnetized and the electron current driven across the magnetic field diverts from the applied electric field direction to the *ExB* direction, which is known as "Hall Effect". This azimuthal drift is thus called "Hall current" and gives the name to the thruster [5,6]. This effect is the basis for the Hall

thruster operation and design, because the electron residence time and propellant ionization in the channel are increased by the Hall motion. As already mentioned, since the ions have larger particle mass, they remained unmagnetized, and the axial electric field accelerates them out of the channel to generate thrust [4].

There are two types of Hall Effect Thruster in the literature: (1) “Stationary Plasma Thruster (SPT)”, (2) “Thruster with Anode Layer (TAL)”. These thrusters are classified according to the material used in their discharge channel. In the case of SPTs, the anode which is electrically biased is positioned at the base of the discharge channel. The wall of the discharge channel is typically manufactured from dielectric materials such as boron nitride (BN) or borosil (BN-SiO_2) due to their low sputtering yield and relatively low secondary electron emission coefficients under Xenon ion bombardment. In the case of TALs, the dielectric channel wall is replaced by a metallic conducting wall [1].

CHAPTER 3

BASICS OF PLASMA DIAGNOSTICS

Various diagnostic systems are used to study the plasma in the plume of a thruster. Different test equipment measures different plasma parameters in such experiments, including plasma potential, electron temperature, electron density, and ion energy distribution. In this section, common plasma probes applied in Hall thruster analysis, i.e., a Faraday Probe, an emissive probe, a retarding potential analyzer, and a Langmuir probe, are introduced to provide an overview of plasma diagnostics and then, Langmuir Probe theory is explained in detail. But first, the definition and properties of plasma are described very briefly below.

3.1 Plasma Definition

Plasma, simply put as an ionized gas, is defined as the forth state of matter as it exhibits distinct features than the other three states of matter. As already explained in the previous sections, in electric propulsion devices, a gas of charged particles needed to be generated and electrostatically accelerated to high velocities to generate thrust with high specific impulse. These charged particles are created from neutral atoms by means of electron collisions in the thruster discharge channel and plasma (ionized gas) is formed consisting of both ions and electrons. It is almost electrically neutral everywhere (i.e., the ion and electron densities are nearly equal, $n_i=n_e$, which is called "quasi-neutrality") except at regions close to the boundaries. In this plasma, ions and electrons typically have different energy distributions and different temperatures (T_i and T_e, respectively) [1].

Plasmas are also classified as "*fully ionized plasma*" and "*weakly ionized plasma*" according to their ionization degree and thus the dominating particle interactions in them. In weakly ionized plasmas, alike particle-collisions are slight and can be

neglected, however, elastic collisions with neutrals are significantly high to dominate the plasma dynamics [21].

Plasmas in different types of electric propulsion devices have distinct distribution of plasma density, temperature, and ionization fraction. Therefore, different assumptions are valid to describe the plasma dynamics in different devices according to the regime being studied [1]. Quasi-neutrality throughout the acceleration region and in the plume of Hall thrusters, for instance, provides a much higher density of accelerated current when compared to ion thrusters [4].

As already mentioned in the previous paragraphs, plasmas can be treated as being electrically neutral (defined as quasi-neutral) depending on their density and temperature. The distance over which quasi-neutrality is violated is often described by the *Debye Length*. Debye Length arises naturally and varies according to the physical characteristics of the plasma. The layer which has a thickness comparable to Debye Length is defined as Debye Sheath [8]. Debye Length is expressed as

$$\lambda_D = \sqrt{\frac{\varepsilon_0 \mathrm{K} T_e}{n_e q_e^2}}, \tag{3.1}$$

where ε_0 is the permittivity of free space, K is the Boltzmann constant, T_e is the temperature of e's, n_e is the density of electrons, q_e is the charge of electrons.

A large number of collisions between charged particles with each other, and the other species take place in the plasma thrusters. In order to evaluate the performance and lifetime of these devices, the dominating plasma dynamics in the device operation must be understood. In most cases, it is not necessary to analyze the motion of individual particles. Instead, different velocity distribution functions are used to describe the macroscopic picture of the plasma processes. A group of particles in thermal equilibrium tends to evolve to a special distribution called *Maxwellian* distribution, which is introduced in the following subsection [1].

3.2 Maxwellian Distribution and Temperature

A group of particles throughout a plasma space under no external disturbance tend to reach thermal equilibrium due to particle collisions. Maxwellian Distribution Theory is used to describe such distribution of particles by a distribution function: this distribution function gives the local number density of the plasma at each spatial point within the defined space if the gas reaches thermodynamic equilibrium [9].

One-dimensional Maxwellian distribution of particles is given below and plotted in Figure 3.1 [8]:

$$f(u) = A\, exp(-\frac{1}{2}\, m\, u^2/KT\,), \tag{3.2}$$

where *f du* is the number of particles per m^3, *A* is a constant to be explained below, *m* is the mass per gas molecule, *u* is the velocity, *K* is Boltzmann's constant, and *T* is the temperature.

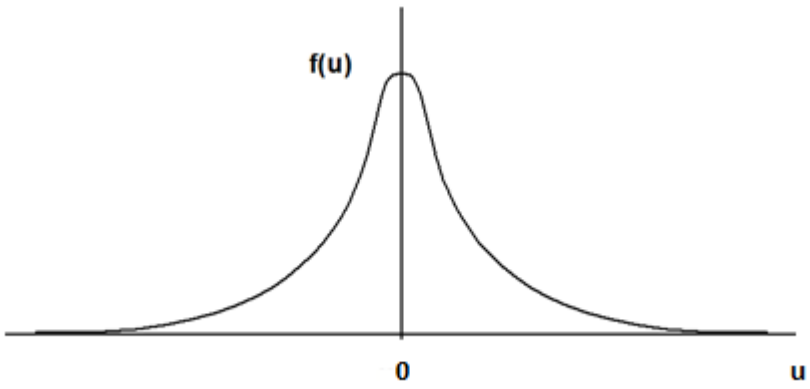

Figure 3.1: 1D Maxwellian distribution [8]

Summary of Chen's derivation in [8] of temperature within a one dimensional Maxwellian distribution of particles is as follows.

The density *n*, or number of particles per m^3, is given by

$$n = \int_{-\infty}^{\infty} f(u)du. \tag{3.3}$$

The constant, *A*, in Eq. (3.2) can be expressed as the function of density distribution as follows:

$$A = n\left(\frac{m}{2\pi KT}\right)^{\frac{1}{2}}. \tag{3.4}$$

In this equation, the constant, *T*, is the temperature and characterizes the width of the velocity distribution, *f(u)*. In order to understand the exact meaning of *T*, the average kinetic energy of particles in this distribution should be calculated:

$$E_{av} = \frac{\int_{-\infty}^{\infty} \frac{1}{2} m u^2 f(u) du}{\int_{-\infty}^{\infty} f(u) du}. \tag{3.5}$$

Defining v_{th} and y as $v_{th}=\sqrt{\frac{2KT}{m}}$ and $y = u/vth$ Eqn. (3.2) can be written as

$$f(u) = Aexp\left(-u^2/v_{th}^2\right). \tag{3.6}$$

Then, Eqn. (3.5) is written in the new form as in Eqn. (3.7)

$$E_{av} = \frac{\frac{1}{2} m A v_{th}^3 \int_{-\infty}^{\infty} [exp(-y^2)] y^2 dy}{A v_{th} \int_{-\infty}^{\infty} exp(-y^2) dy}. \tag{3.7}$$

Taking the integrals in Eq. (3.7) gives the average kinetic energy for a group of particles in a 1D Maxwellian distribution, $E_{av.}$ The average kinetic energy is defined as

$$E_{av} = \frac{1}{4} m v_{th}^2 = \frac{1}{2} KT. \tag{3.8}$$

In order to derive the average kinetic energy in three-dimensions, a similar process can be applied using the three-dimensional Maxwellian distribution, which is defined as

$$f(u,v,w) = A_3 exp\left[-\frac{1}{2}m(u^2+v^2+w^2)/KT\right], \tag{3.9}$$

where

$$A = n\left(\frac{m}{2\pi KT}\right)^{\frac{3}{2}}. \tag{3.10}$$

If we skip through all the mathematical steps, we can then write the average kinetic energy for a three-dimensional Maxwellian distribution as

$$E_{av} = \frac{3}{2}KT. \tag{3.11}$$

The results show that T and E_{av} are closely related in plasma under thermal equilibrium. Therefore in plasma physics the temperature is defined in units of energy, eV. Also, KT is used to denote the temperature, where 1 eV is equal to $1.6\text{x}10^{-19}J$, i.e., $KT=1eV=1.6\text{x}10^{-19}J$.

3.3 Probe Types

3.3.1 Faraday Probe

Faraday probe is a diagnostic tool which is used to measure ion current density distribution of plasma. It has a flat metal plate, called “collector”, which is exposed to a plasma flow as seen in Figure 3.2. In plasma applications, the collector is generally made of stainless steel and sprayed with tungsten [11]. The ion flux into the probe surface generates the probe current which is recorded and divided by the surface area to measure the ion current density. The probe is biased to a suitably large negative potential with respect to the local plasma potential to repel all the electrons and therefore collected current consists of only ions [5].

An example photo of Faraday probe is shown below. While the principle and implementation of Faraday probe is simple, accurate interpretation of the measurements is usually difficult and requires careful analysis [10].

Figure 3.2: Photograph of Faraday Probe [12]

3.3.2 Emissive Probe

Emissive probe is a diagnostic instrument for determining the plasma potential in plasmas [13]. In this type of probe, there is a small loop of tungsten wire passed through a double-bore ceramic tube as shown in the figure below [11].

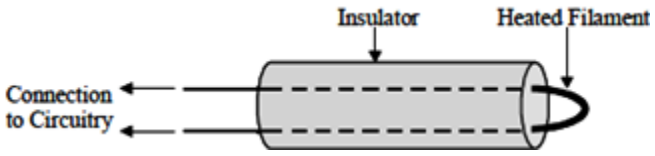

Figure 3.3: Schematic of Emissive probe [10]

As seen in the figure, an external current source is used to heat the tungsten filament and to trigger the emission of electrons. Electron current that floats to the local plasma potential can then be directly measured. The important point in the design of

this type of probe is that the probe must be biased negatively with respect to the plasma potential for the initiation of the electron emissions as electrons travel up the potential gradients. While other type electrostatic probes need a voltage sweep or data reduction, the emissive probe gives a direct measure of plasma potential which is the major advantage of this type of instrument [14, 11].

3.3.3 Retarding Potential Analyzer

A Retarding Potential Analyzer (RPA) is a diagnostic element that measures current density and ion energy of plasma distribution using a series of grids to selectively filter ions. Biased grids shield a current collector in it which varies as a function of the ion retarding electrode potential. While the use of RPA is easy, the design of it is challenging [11, 15]. As you see in the Figure 3.4, RPA is a flat gridded probe in which a series of electrodes separated and insulated [15].

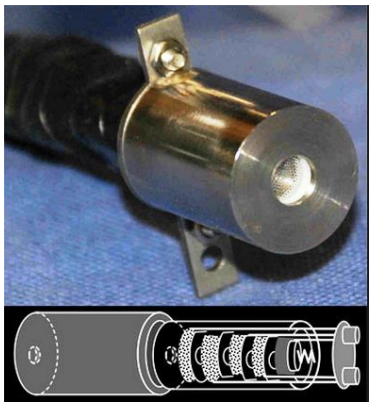

Figure 3.4: Retarding Potential Analyzer [15]

3.3.4 Langmuir Probe

Langmuir probe, invented by Irving Langmuir in 1924, is an electrostatic diagnostic tool used in the evaluation of several plasma properties (see Figure 3.5). A Langmuir probe is basically just a wire inserted into plasma to collect electron and/or positive ion currents by applying a bias voltage to it as shown in Figure 3.6. In low

temperature plasmas, local plasma potential, electron number density and electron temperature can be measured by Langmuir Probes [4, 16].

Langmuir probes are classified according to their shape as spherical, planar and cylindrical and according to their electrode number as single, double, triple and even quadruple [4]. A Single Langmuir Probe consisting of a single cylindrical electrode is operated by connecting it to an external biased voltage and changing the probe voltage with respect to the local plasma. The plot of collected current by the probe with respect to bias voltage gives the current-voltage characteristics of the probe (simply called I-V curve), an example of which is given in Figure 3.7.

Figure 3.5: A single Langmuir Probe

Local plasma potential, electron number density, and electron temperature can be discerned from this current-voltage characteristics [17, 4] Taking current data by the probe with respect to bias voltage is easy; however, analyzing and deriving the results from the current-voltage (*I-V*) curve reliably is quite complicated due to the disturbed plasma effects [17].

3.4 The Langmuir Probe Theory

Although the Langmuir Probe has a simple structure and the construction of it is relatively easy, the physics behind its operation is quite complicated and reliable evaluation of measurements requires tedious analysis. Therefore, as a result of several years of work and experience, a Langmuir Probe theory was established for easier interpretation of the *I-V* curve and determination of the plasma parameters using these probes. Langmuir probe theory is included in the following paragraphs.

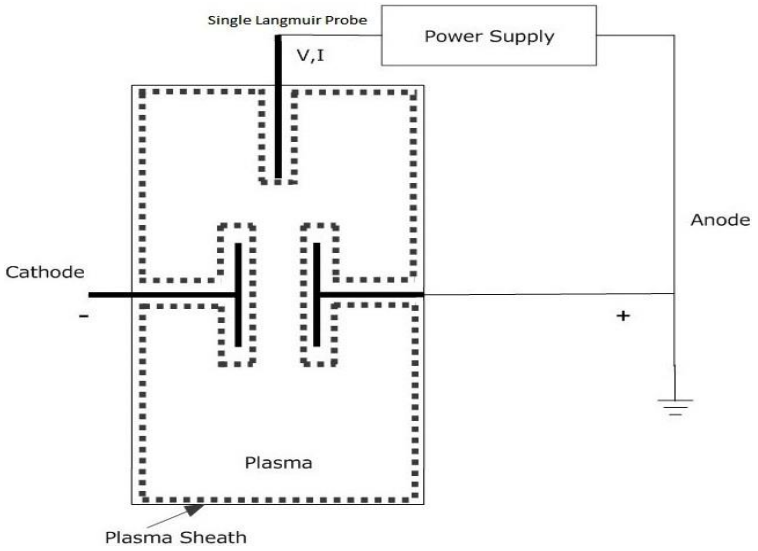

Figure 3.6: Single Langmuir probe placed into the plasma [18]

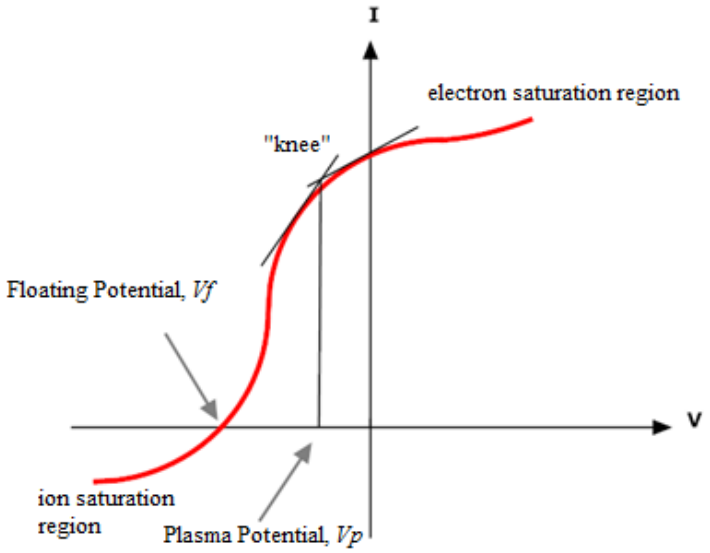

Figure 3.7: A typical plasma current-probe voltage characteristic graph of a Langmuir cylindrical probe [18]

Figure 3.6 shows a Single Langmuir Probe placed into plasma and Figure 3.7 shows an example of a typical *I-V* curve that can be obtained from the probe. As seen in the *I-V* curve, there are three main regions called as "*ion saturation"*, "*electron retardation (transition region)"* and "*electron saturation*" to be analyzed. *Ion*

saturation region occurs at the left hand side of floating potential "V_f" at which ion and electron currents reach a balance and the collected net current is zero. For very negative bias voltages, electrons are repelled from the probe but ions are attracted by the probe, so collected current is dominated by the ions and ion saturation current, I_{sat}, is formed.

In *electron retardation region*, which is the *transition region*, when the probe bias voltage is increased by applying less negative values, electrons continue to be pushed and only the highly energetic electrons are able to pass the sheath to make contribution to the collected current and there is a positive current towards the electrode. In this region, the probe collects both positive ions and energetic electrons but the electron current is more dominant than the ion current because the electrons move faster than the ions due to having lighter mass [38]. When the probe bias voltage is further increased, local plasma potential bends over a knee-point [4] (marked in Figure 3.7). This part of the curve is exponential in Maxwellian plasma. The exponential growth of I_e with V should continue until probe potential becomes equal to plasma potential, i.e., $V=V_p$ [22]. Plasma potential is observed near the "knee" point and can be obtained using the maximum of the first derivative of the probe characteristic as will be described in more detail in the following section.

When the probe potential is greater than the plasma potential, $V>V_p$, sheath forms by expanding the collecting area so the probe current increases slightly in this region [18]. Sheath occurs around the probe in plasma in order to maintain charge neutrality in the bulk of the plasma. Sheath expands and saturation currents increase gradually with increasing bias voltage [16], which is observed as the positive slope in the *I-V* curve in Figure 3.7

Sheath expansion changes depending on the plasma density and probes' area. For lower plasma densities and small probes, because the effective area for particle collection is the sheath instead of the probe area, the sheath expansion produces an increase in the collected current. As the sheath expands, some particles can enter the sheath and some plasma particles could not be collected by the probe. As the bias voltage is increased, more particles will be collected [16].

In *electron saturation region*, an increase in the biased voltage beyond the knee point results in electron saturation and almost all electrons are collected by probe. In this region, the sheath becomes even thicker [4]. As the probe voltage is increased, the electron current with thermal motion moves through the constant sheath region, so the electron current is saturated. Because the electron velocities are $\approx(m/M)^{1/2}$ times larger than ion velocities, electron saturation current, $I_{es,}$ is much larger than ion saturation current, I_{sat}. When the bias voltage increases in this region, I_e increases slowly and sheath expands so the collection area grows, resulting in the slight positive slope in the right most part of the I-V curve in Figure 3.7 [22].

3.4.1 Analyzing the Current-Voltage Characteristics of a Langmuir Probe

Assuming a Maxwellian distribution for the electrons in the plasma, plasma potential (V_p), electron temperature (T_e), and plasma density (n_e) can be derived from the I-V characteristics by the standard Langmuir probe theory assuming that the probe operates in the collisionless regime.

First, in order to obtain the plasma potential, the point where I_e starts to deviate from exponential growth is used. Plasma potential V_p is the value when $I_e'(V)$ (first derivative of the current) is maximum or $I_e''(V)$ (second derivative of the current) is zero [22]. In order to measure plasma potential, the maximum of the first derivative of the probe characteristics is obtained [19].

Second, electron temperature, T_e, can be obtained from the IV curve using the data in the transition region. In this region, if the electrons are Maxwellian, the electron current can be expressed as [22],

$$I_e = I_{es} exp\left[e(V - V_p)/KT_e\right]. \tag{3.12}$$

The electron saturation current, I_{es}, is given by

$$I_{es} = \frac{1}{4} e n_e v_{e,th} A_{probe}, \tag{3.13}$$

where n_e is the electron density, A_{probe} is the exposed area of the probe tip, m_e is the electron mass, $v_{e,th}$ is the electron thermal speed [16],

$$v_{e,th} = \sqrt{8KT_e/\pi m_e}. \tag{3.14}$$

$$A_{probe} = 2\pi r_p l. \tag{3.15}$$

Eqn. (3.12) shows that the slope of the $(\ln I_e) - V$ gives exactly $1/KT_e$ [22] in eV.

Therefore when the exponential part of the *I-V* curve in this transition region is plotted semi-logarithmically with respect to the probe voltage *V*, the result should be a straight line. In other words, Eqn. (3.12) shows that the slope of the $\ln I_e$ with respect to *V* gives exactly $1/KT_e$ in eV [22]. Thus, electron temperature is obtained easily from the slope of the logarithm of the electron current in the transition region as follows,

$$KT_e = \left(\frac{d\ln I_e}{dV}\right)^{-1}. \tag{3.16}$$

Third, electron number density (assuming quasi neutrality, it is equal to plasma density) can be derived from the ion-saturation current region. Typically ion-saturation current is preferred to be used in the calculation of electron number density because the ion-saturation currents are much smaller and easier to handle due to the low output impedance when compared to electron-saturation currents [22].

Calculation of electron density is not as straightforward as the temperature and plasma potential as given above. In the interpretation of I_{sat}, different theories can be applied for ion collection according to properties of the plasma and the structure of the probe with respect to the plasma properties. Usually, a collisionless sheath around the probe is assumed by currently accepted theories that are used in the analysis of low pressure laboratory plasmas [43]. The general orbital motion (OM) theory of Laframboise (1966) follows this approach and this theory is reduced to the

orbital motion limited (OML) regime by Allen in 1992. For cylindrical probe geometry, another approach is proposed by Chen (ABR-Chen) in 1965, which is called "the cold ion radial motion theory". Due to this variety of approaches, disagreements in plasma density measurements can be commonly seen in the literature between these different collisionless probe theories (e.g. OML, ABR-Chen) and independent methods such as microwave interferometry (Sonin 1966, Sudit and Woods 1994, Chen 2001). Moreover, Su and Kiel in 1966 and later Cohen in 1967 studied and formulated the current-voltage characteristic in the *thin sheath limit*. *The thick sheath limit*, however, is expressed by Chang and Laframboise in 1976 for the probe currents, assuming the potential in the vicinity of the probe is given by Laplace's equation for vacua [43].

In summary, for cylindrical probes, two fundamental approaches (extremities) applied in the interpretation of the I_{sat} curve include "Thin Sheath Analysis (Bohm Ion Saturation Current Model)" and "Thick Sheath (Orbital Motion Limited, shortly OML) analysis". Derivations of ion current for these analyses are given in Appendix and only brief summaries of the results will be discussed for the sake of simplicity in the section.

3.4.2 Thin Sheath Analysis

In ion saturation region, bias voltage on the probe, V, is sufficiently negative with respect to the plasma potential, V_p, so the ion dominated current, I_{sat}, is collected by the probe. In this region, a thin sheath around the probe occurs when the ratio of probe radius to Debye length is greater than or equal to 10, which is usually occur in high density plasmas [17]. When thin sheath case is observed, the current collection of the probe is limited by the electric field within the sheath, which is called as "space charge limited" current [9]. For ion-attracting probes, electric fields in the quasi-neutral plasma outside the sheath accelerate ions with a velocity of $(KT_e/m_i)^{1/2}$ where m_i is ion mass. In order to have a stable sheath, ions must reach the Bohm velocity [17]. Therefore, in "Thin Sheath Analysis", the ion-saturation current is expressed by the Bohm Ion current [5]:

$$I_{sat} = I_{Bohm} = 0.6en_i\sqrt{\frac{KT_e}{m_i}}A_{probe}. \quad (3.17)$$

Because of the quasi-neutrality, n_e=n_i=n, so n_e can be calculated by

$$n_e = \frac{I_{sat}}{0.6e\sqrt{\frac{KT_e}{m_i}}A_{probe}}. \quad (3.18)$$

3.4.3 Orbital Motion Limited (OML) Analysis

In the low density regime, for ion collection, the Orbital Motion Limited (OML) theory is commonly applicable in the industry [44]. In such cases, the ratio of probe radius to Debye length is smaller than or equal to 3. According to "Thick Sheath (Orbital Motion Limited, shortly OML) analysis, electron number density (assuming quasi neutrality, it is equal to plasma density) can be derived from the following approximate formula for the ion-saturation current [20]:

$$I_{sat} = A_{probe}n_e\frac{\sqrt{2}}{\pi}\sqrt{\frac{e(V_{s1}-V)}{m_i}}, \quad (3.19)$$

$$n_e = \frac{I_{sat}}{A_{probe}\sqrt{\frac{e(V_{s1}-V)}{m_i}}}\frac{\pi}{\sqrt{2}}, \quad (3.20)$$

where V_{s1} is a *temporary* plasma potential used for fitting [20].

Note that this formula does not depend on KT_e, therefore, n_e can be determined by fitting a straight line to the slope of the I^2-V plot [39]. In other words, in OML regime, the electron density is calculated from the slope of I^2 versus V plot, which is proportional to n_e^2 [19].

In our study, for the reasons that will be explained in the following chapter, "thick sheath analysis assumption" (i.e., OML) is used (see Section 4.3).

CHAPTER 4

PROBE DESIGN AND MANUFACTURE

In this section, Langmuir probe design methodology and criteria are introduced briefly and their application to our design is discussed in detail.

4.1 Design Criteria

As already introduced in the previous section, plasmas are classified as "*fully ionized plasma*" and "*weakly ionized plasma*" according to their ionization degree and also classified as *"collisional"* and *"collisionless"* according to their number density [21]. These classifications determine the main characteristics of the plasma behavior. In this study, we consider weakly-ionized discharges in which elastic collisions with neutrals and charge-exchange interactions are dominant.

In probe design, (1) the length scale of plasma (Debye Length), (2) Knudsen Number and (3) probe geometry are three important parameters that need to be considered simultaneously. Results from the analysis of these parameters provide information to identify the approach for the evaluation of the I-V characteristics and derive the governing formulas from the curve for parameter determination.

In chapter (3.1) we already introduced the Debye Length. Knudsen number (Kn) is a dimensionless parameter that characterizes the particle collisions in the probe sheath [4]. A term, *mean-free path*, λ_{mfp}, which measures the typical distance a particle travels between "collisions" should be introduced to define the *Knudsen Number*. Then, Knudsen Number [Kn] can be expressed as the ratio of *mean free path* (λ_{mfp}) to the *probe radius* (r_p) [4]:

$$K_n = \frac{\lambda_{mfp}}{r_p}. \tag{4.1}$$

If the electron-neutral mean-free path, (λ_{mfp}), is greater than the probe radius (r_p), the Knudsen Number, (K_n), is greater than unity which indicates that the probe operates in a collisionless regime. If the Knudsen Number is less than unity, that means the probe is in collisional regime [4].Therefore, Knudsen number is the first parameter that needs to be considered both in the design of the probe and then in the analysis of the probe measurements. Physically this number indicates whether there are too many collisions in the probe sheath or they are sufficiently low that they can be ignored [22, 4].

The geometry of the probe is also an important parameter for determination of the plasma parameters [22]. The shape of the probe affects sheath thickness in plasma and therefore determines the approach for the interpretation (Thin sheath or OML) of the plasma density measurements. Typically cylindrical probes are used in the literature for their relatively simple manufacture and analysis. All analysis formulas and equations give in this study based on this shape. In addition to shape, the number of electrodes is important, which range from 1 to 4 in the applications in the literature. The ratio of the probe radius to the Debye Length is the final geometry parameter in the Langmuir probe design. As already explained previously, thickness of the plasma sheath formed around the probe is proportional to the Debye Length. Debye length is defined as

$$\lambda_D = 7430\left(KT/n\right)^{1/2}, \qquad (4.2)$$

where n is plasma density in m^{-3}, KT is electron temperature in eV, λ_D is Debye length in m. The relationship between the probe radius and Debye Length is specifically important while evaluating the alternative probe geometries and then the theories that can be applied in the interpretation of the measurements. Thin sheath and thick sheath analysis (OML) in the Langmuir Probe Theory described in Chapter 3 have been developed based on the relationship between the Debye Length and probe radius [9]. If the ratio of probe radius to Debye Length is smaller than ~3, it can be said that probe is in *thick sheath region* but, if that is bigger than ~10, *thin sheath analysis* can be applied [4].

In the Table 4.1, a number of probe dimensions used in the Hall Effect thruster experiments are listed from the literature. These probes are designed taking into account the criteria mentioned above for plasma measurements in the performance tests of different Hall Effect Thrusters. As will be seen in Figure 6.1, since the plasma characteristics vary substantially in different regions with respect to the discharge channel of Hall Effect thrusters, three main regions are defined for the plasma analysis. These regions are called "inside the channel", "very near field" and "far field". For SPT-100s, the region from 10 mm to 200 mm downstream of the thruster exit plane is called "very near field" and the region from 25 cm to 1 m downstream of the thruster exit plane is called "far-field", which require separate approaches in the determination of the plasma parameters in the SPT-100s operation [5]. In other words, as the plasma properties are different inside the thruster, in the near field, and far field, different measurement methodology and Langmuir probes geometry with different characteristics are needed to be used. Different Langmuir probe examples that are used in the SPT 100 experiments in different regions are given for comparison in Table 4.1 below.

Table 4.1 Examples for Langmuir probes used in the SPT 100 tests in the literature

Field of measure.	**Thruster Type**	**Probe Materials**	**Probe Diameter**	**Probe Length**	**Coating Type**
Very Near	SPT100 [5]	Tungsten wire	0.127 mm	0.88 mm	Alumina
Far	SPT 100 [4]	Tungsten wire	0.5 mm	10 mm	Alumina
Near	SPT100-ML [23]	Tungsten wire	2 mm	20 mm	Alumina
Far	PPS100-ML[18]	Tungsten wire	0.38 mm	100 mm	Alumina with 2mm diameter

4.2 Probe Dimensions and Materials

In order to protect the probe erosion due to the plasma flow, a high-temperature resistant material, usually a tungsten rod or wire, are used for the probe tip in the literature: thicker the wires better the resistance of the probe to erosion. In addition to this, a ceramic tube is used to coat the wire for further protection. On the other hand, to avoid disturbance of the plasma, a thin ceramic coating, preferably less than 1 mm in diameter, is chosen for insulation [22]. To meet this criterion, the probe wire needs to be selected as thin as possible. Therefore, in the literature usually a tungsten wire with a diameter ranging from 0.1 mm to 1 mm and a length ranging from 2 mm to10 mm and a suitable ceramic coating are used (also refer to Table 4.1).

4.3 Details of Our Design

In this work, a tungsten wire with a diameter of 0.375 mm and length of 11 mm is used. Total length of the probe is determined 32.5 cm. As seen in Figure 4.1, for both probe protection and avoid of plasma disturbances, a ceramic coating is also utilized as plotted in Figure 4.1.

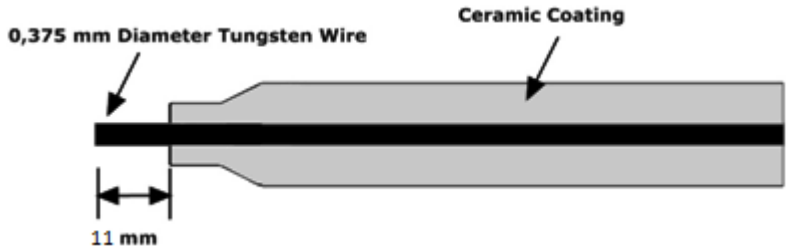

Figure 4.1: General view of single Langmuir probe [5]

In Figure 4.2, the 3D drawing of the designed Single Langmuir probe is given and the physical dimensions of the probe summarized in Table 4.2

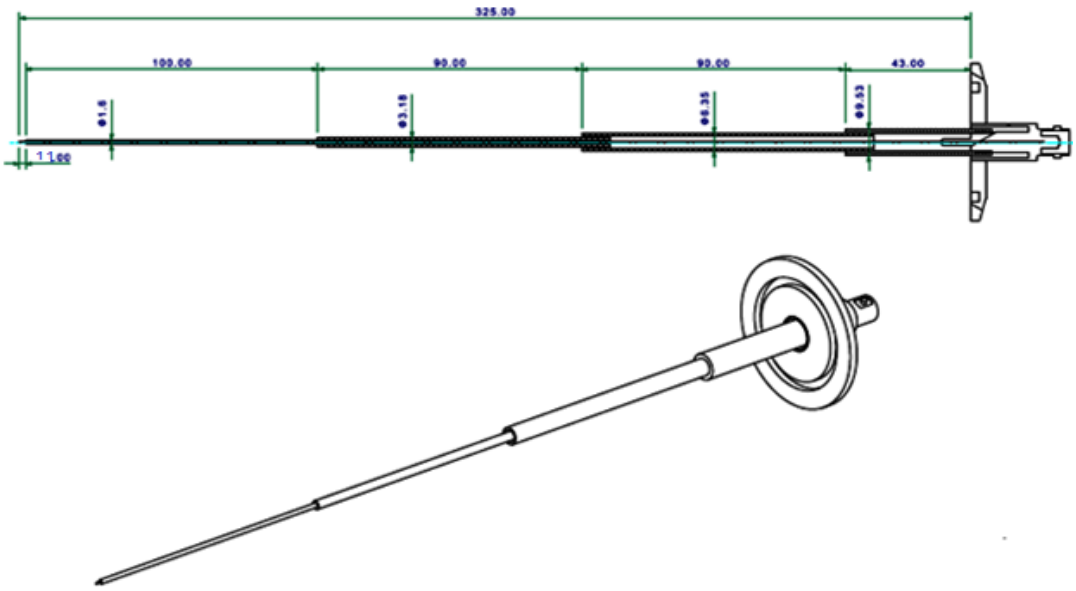

Figure 4.2: 3D drawing of the designed Langmuir Probe

Table 4.2: The physical dimensions of the single Langmuir probe

Parameter (unit)	**Value**
Tungsten wire diameter (mm)	0.375
Tungsten wire length (mm)	11
Ceramic coatings diameters (width-length) (mm)	1.6-100, 3.18-90, 6.35-90, 9.53-43
Total length of the Langmuir probe (mm)	325

Analysis of Important Plasma Parameters for Our Design

In order to determine whether OML (thick sheath) or thin sheath analysis is applicable in our design, some important plasma parameters are calculated using typical plasma values for low pressure discharges.

Debye length is described by eqn. (4.2),

$$\lambda_D = 7430\left(KT/n\right)^{1/2}.$$

Range of typical parameters for low pressure discharges [24] is listed in Table 4.3:

Table 4.3 Range of typical plasma parameters for low pressure discharges

Typical Plasma Parameters for low pressure	Min	Max
Electron temperature, *KT* (eV)	1	10
Pressure, *P*, (Torr)	0,1	1
Plasma density, *n*, (m^{-3})	10^{14}	10^{19}

The ratio of the probe radius to Debye Length is an important design criterion as mentioned before. Below, we calculated this ratio for two limiting cases of the temperature and density:

For $KT = 1eV,$
$n_e = 10^{19}m^{-3}.$

Then, Debye length is,

$$\lambda_D = 7430\left(\frac{1}{10^{19}}\right)^{\frac{1}{2}} = 2.35x10^{-6}m = 2.35x10^{-3}mm.$$

As our Langmuir probe radius is 0.188 mm, the ratio of probe radius to Debye length (r_p/λ_D) is 80>10 and the probe works in thin sheath region for this case.

For $KT = 10eV,$
$n_e = 10^{14}m^{-3},$

we have

$$\lambda_D = 7430\left(\frac{10}{10^{14}}\right)^{\frac{1}{2}} = 2.35x10^{-3}m = 2.35mm.$$

Again as our Langmuir probe radius is 0.188 mm, the ratio of probe radius to Debye length (r_p/λ_D) is 0.08 < 3.

Therefore, the probe works in OML regime and thick sheath analysis is applicable for this case.

To summarize, we listed the calculated parameters in Table 4.4. Our probe has a diameter of 0.188 mm and length of 11 mm and therefore it can work in both thick (OML) and thin sheath regimes in a low-pressure discharge plasma having parameters within the limits given in Table 4.3. In Chapter 7, however, further discussion on the plasma parameters will show that our probe operates in collisionless regime and thick sheath (OML) theory is applied in the analysis of our probe's measurements obtained in the RF plasma generated at METU Physics Plasma Laboratory.

Table 4.4 Summary of calculated plasma parameters for two different plasma properties

Parameters	**For low n_e, high KT**	**For high n_e, low KT**	**Equations used**
Debye Length(mm)	$2.35x10^{-3}$	2.35	$\lambda_D = 7430\left(KT/n\right)^{1/2}$
Ratio of Radius of probe to Debye Length	80 * Thin sheath analysis is applicable	0.08 * OML analysis is applicable	r_p/λ_D $r_p = 0.1875mm$

CHAPTER 5

MANUFACTURING OF THE PROBE

5.1 Probe Materials

In this chapter, materials which were used in the production of the designed Langmuir probe are introduced in detail. These materials were chosen examining the similar probe applications in the literature.

5.1.1 Tungsten Wire

Tungsten, also known as wolfram, has high density and the highest melting point of all the elements. Also, tungsten has a very low secondary electron yield [11]. Because of its high melting point and very low secondary electron yield, the probes are commonly constructed with tungsten in order to protect the probe from the plasma and also not disrupt the plasma. As seen in Table 4.1, in Hall thruster applications, tungsten is generally preferred for the probe tip construction. Therefore, in our design for the probe tip, we also used tungsten wire which is 0.375 mm in diameter and 11 mm in length.

5.1.2 Ceramic Coating

Ceramic materials can be defined as inorganic, non-metallic, heat-resistant solids. Generally, they are highly resistant to corrosion and hard, but brittle. Ceramic materials can be used with other materials, generally, for coating on [26]. Thin and thick coatings can be applied depending on the functional applications. Ceramic tubes with varying thickness and diameters are used in our Langmuir probe for the coating of the tungsten wire in order not to disturb the plasma and get precise results. Our probe design consists of four ceramic tubes in different sizes, which are already given in the previous chapter (see Figure 5.1).

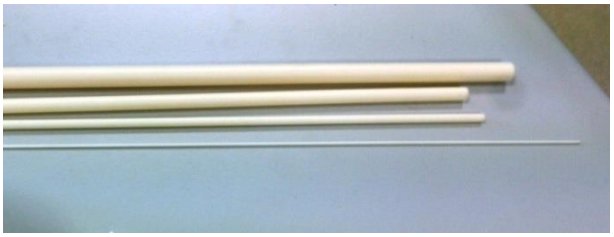

Figure 5.1: Ceramic tubes used for the probe wire coating

5.1.3 QF Flange (QF to Test Port)

In vacuum applications, in order to transfer the Langmuir probe from outside of the vacuum chamber to inside while maintaining vacuum is a critical issue. For this purpose, an electrical vacuum feed through is utilized, which is a flange that contains a vacuum-tight electrical connection to the vacuum chamber allowing voltages applications.

ISO (International Standard Organization) flanges along with QF (Quick Flange), LF (Large Flange), A&N ISO flanges and CF flanges are most commonly used vacuum flanges in high vacuum systems. All these flange types are offered in a range of dimensions [27]. For our experimental set up, standard QF flanges which have tube sizes ranging from 16 mm to 50 mm (QF16 to QF50) can be used on the vacuum chamber [28].

QF40 flange by Kurt J. Lesker Company is determined to be used to feed through our probe to the vacuum chamber. This flange has BNC coaxial connectors on the air-side and the connector-plug pair's impedance is (unmatched) 48-52 ohms (matched 50 ohm pairs are available). The alumina insulated conductor is rated at 500V with a grounded shield and at 2500V with a floating shield, at 3A. Also, the QF flange is sealed with centering and O-ring combination (not supplied) making it high vacuum compatible [29]. CAD drawing of the QF 40 flange used can be seen in Figure 5.2.

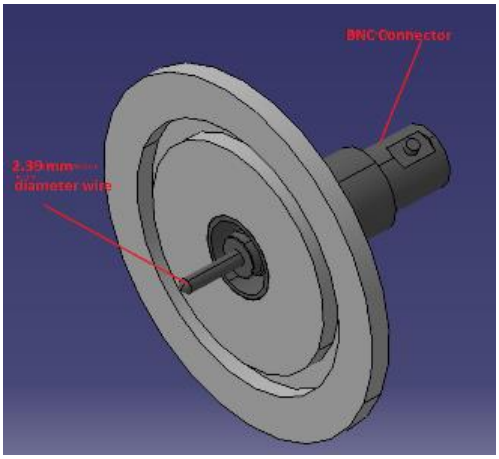

Figure 5.2: CAD drawing of the QF40

Also, push-on connector is used to connect the tungsten wire with 0.375 mm diameter and the wire of QF 40 flange with 2.39 mm diameter. FHP-BECU-2.4-CON is used for our system as seen in the following figure [30].

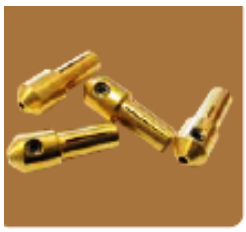

Figure 5.3: BeCu with stainless steel set screws [30]

In the following figure, all the materials used in probe production are illustrated, which are the tungsten wire, ceramic tubes, QF flange and connectors.

Figure 5.4: All materials used in the probe production

5.1.4 Vacuum Epoxy

In order to attach ceramic tubes to each other, Torr Seal vacuum epoxy is used. Torr Seal vacuum epoxy is preferred as it is a sealant used in high vacuum applications and usually used for safe handling. The vacuum epoxy consists of two parts A (resin) and B (hardener) which are mixed in the correct ratio and blended thoroughly until the color and consistency are uniform.

When left at room temperature, after 24 hours, approximately 90% of the full dry properties are attained and after three days the products are completely dried and ready to use. Cure can also be obtained in 1 hour at 82°C or in 20 to 30 minutes at 121°C [31].

Figure 5.5: Torr Seal vacuum epoxy [31]

5.1.5. End Product

Manufacture of the probe was completed within 3 days because drying of epoxy takes time as mentioned before. The bottom three ceramic tubes are fixed to each other and then fixed to the QF flange but the thinnest ceramic tube at the end near the probe tip is left un-fixed. In case of corrosion of the tungsten wire, the wire is needed to be replaced. For easy handling, this end tube is removed and the new wire is inserted into a small clip placed inside this thinnest tube here. The photograph of the end product is shown in Figure 5.6 and 5.7.

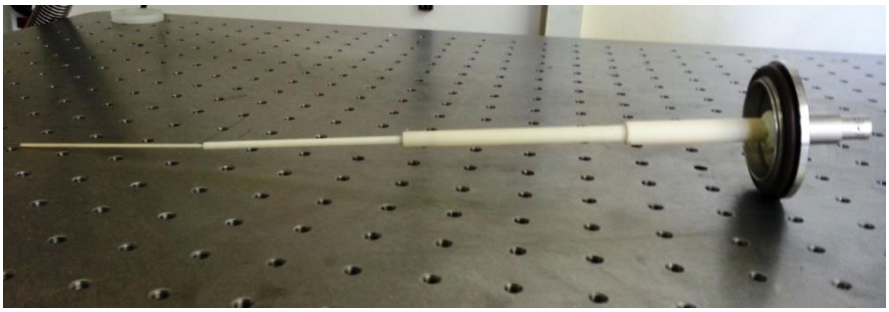

Figure 5.6: The end production of probe

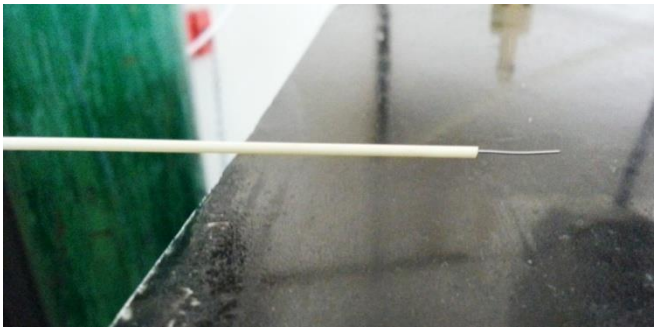

Figure 5.7: The probe tip

5.1.6 Electrical Circuit Design to Derive the Probe

Plasma data from the probe is obtained using the circuit illustrated in Figure 5.8 and Figure 5.9. The circuit consists of a power supply, an oscilloscope, an operational amplifier (opamp) and a shunt resistance. The tungsten electrode is biased relative to tank ground using Keithley 2400 Model SourceMeter, and the probe current is detected across the 10 kΩ resistor using the AD 620 operational amplifier which is a low cost, high accuracy instrumentation. This circuit was designed for DC plasma measurements in Hall Effect Thruster Experiments where typically observed currents are quite small, on the order of micro-amps. Therefore opamp in this circuit is utilized for two proposes by powering it with two 9 V batteries and adjusting its gain by using a BAOTER 3298. The first function of the opamp is to amplify the low current detected on the shunt resistor to a much higher value at the output and the second function is to isolate the measuring device from the circuit to minimize its possible effect on the measurements. However, as the HET experiment setup at TUBITAK UZAY is not ready and the probe is tested in low pressure RF plasma at METU Physics Plasma Laboratory, we use the circuit without utilizing the opamp. The circuit is then put into a metal box as seen in Figure 5.9 to minimize the influence of the environmental low frequency noise on the measurements. In our experiments, the probe is biased by Source Meter by sweeping -10 to +10 and current-voltage characteristics stored in the Source Meter for an analysis in MATLAB.

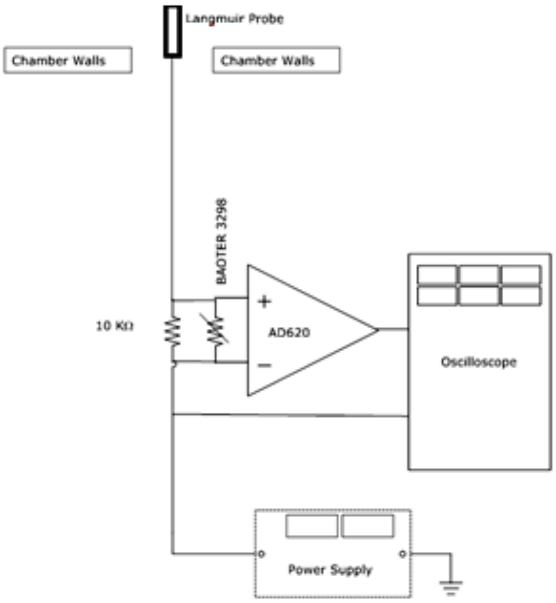

Figure 5.8: Schematic of the probe circuit for HET experiments [5]

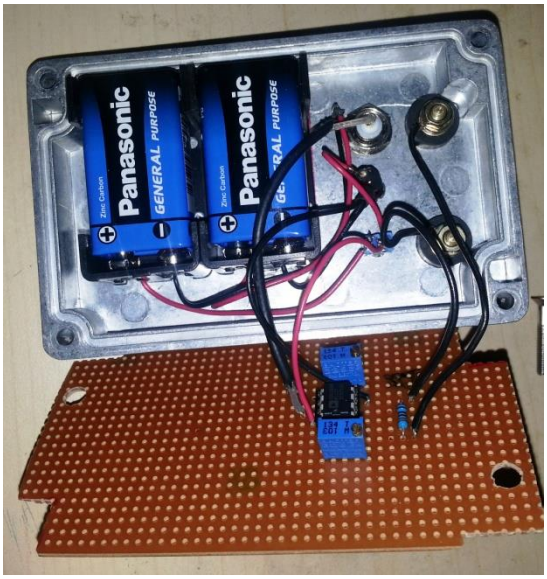

Figure 5.9: The photo of the probe circuit

The schematic of the circuit for HET experiments and the photograph of the circuit and the experimental setup are given in Figure 5.8, 5.9 and 5.10 respectively.

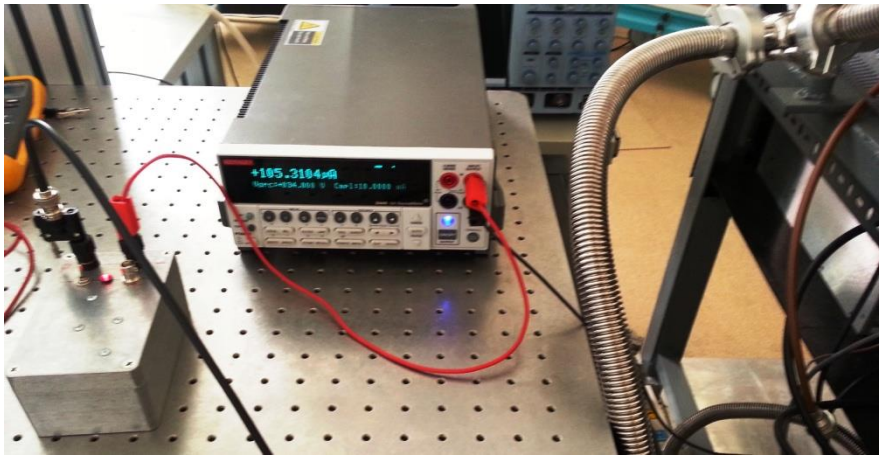

Figure 5.10: Experimental set-up of the circuit

CHAPTER 6

EXPERIMENTAL SET-UP

In general, plasma properties inside, near and far from the thruster vary in great respect (see Figure 6.1). Therefore different measurement methodologies and different Langmuir probe designs are needed to be used in these different regions. As our initial objective in this study was to study the *plasma* parameters in the *far-field* plume of a *Hall Effect thruster, SPT 100 specifically, we designed and manufactured our probe considering the typical characteristics of HET plume plasmas published in the literature.* However, since the Hall Effect Thruster and the vacuum system at TUBITAK UZAY is not yet complete by the submission of this thesis as planned in the beginning of the project, plasma measurements and Langmuir probe tests are needed to be conducted in a small vacuum chamber at the METU Plasma Physics Laboratory instead.

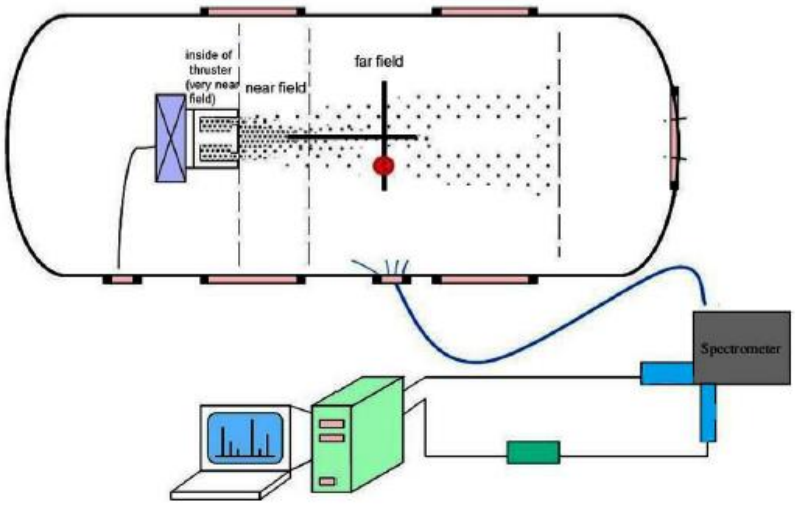

Figure 6.1: Schematic of Experimental Set-up of Hall Effect Thruster, showing different regions of plasma [32]

6.1 Vacuum Chamber

Vacuum chamber system used in the tests of the designed probe is shown in the figure below. Langmuir Probe is inserted into this stainless steel cylindrical plasma chamber, whose height is 500 mm and diameter is 400 mm. Inside the chamber, two identical electrodes are assembled with a 40 mm distance like a parallel plate capacitor. Diameter of these two-isolated identical aluminum electrodes is 200 mm. The plasma is generated by heating the gas between the electrodes under low pressure. In this system, both RF and DC generators can be used as a power source. For our experiments, we use 40.68 MHz RF high Radio Frequency for Power Supply. Moreover, we use 99.995 % purity nitrogen gas is used as an activation gas for diagnostic analysis and the range of nitrogen gas pressure is 0.1-0.5 Torr. Picture of our plasma chamber system and plasma chamber in which the handmade Langmuir probe inserted are given in Figure 6.2 and 6.3, respectively.

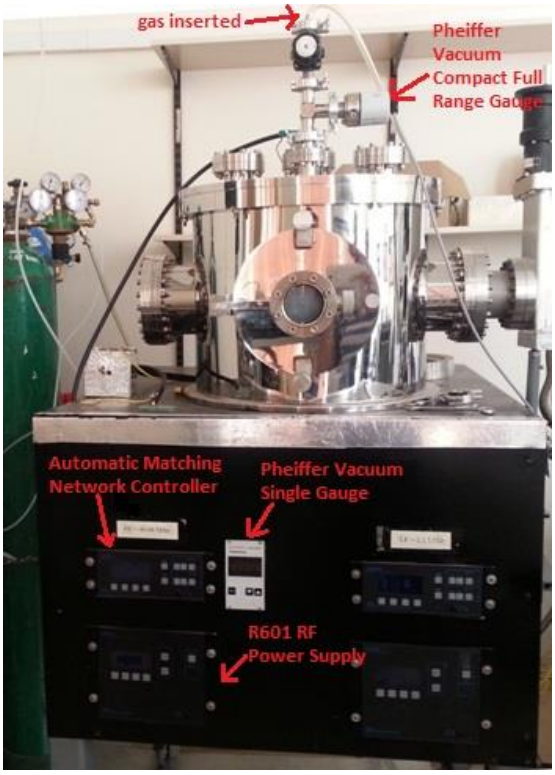

Figure 6.2: Picture of our plasma chamber system

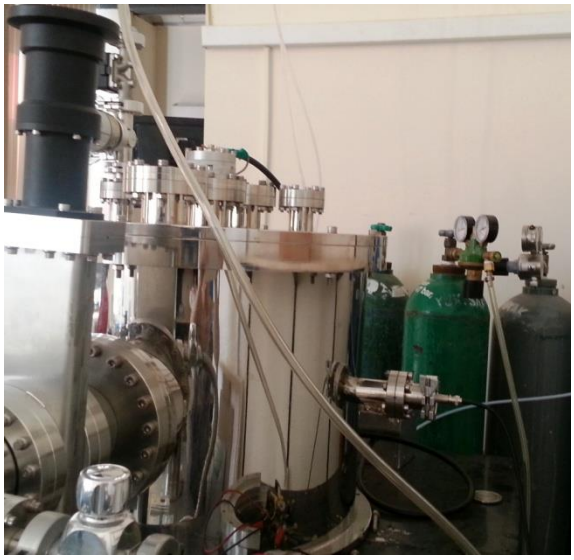

Figure 6.3: Plasma chamber in which the handmade Langmuir probe inserted

Capacitively Coupled RF Plasma is designed by two parallel metal plate electrodes separated by a small distance in a reactor chamber filled with nitrogen. When RF voltage is applied between the electrodes, an oscillating electric field is generated, then the gaseous electrons are accelerated by the means of RF electric field. Electrons collide with gas atoms elastically and inelastically generating new electrons and ions. The electrons are faster than the ions due to their light masses, so, when some of electrons and ions escape from the plasma and move toward the "chamber wall or electrode", electrons can reach it earlier. As soon as electrons arrive the solid body, "chamber wall or electrode", they start to pull the ions toward the solid body and push the other electrodes toward the bulk plasma. Thus the bulk plasma is approximately "quasi-neutral" and the region close to the solid body has more ions [38]. The schematic expression of Capacitively Coupled Plasma is given in Figure 6.4.

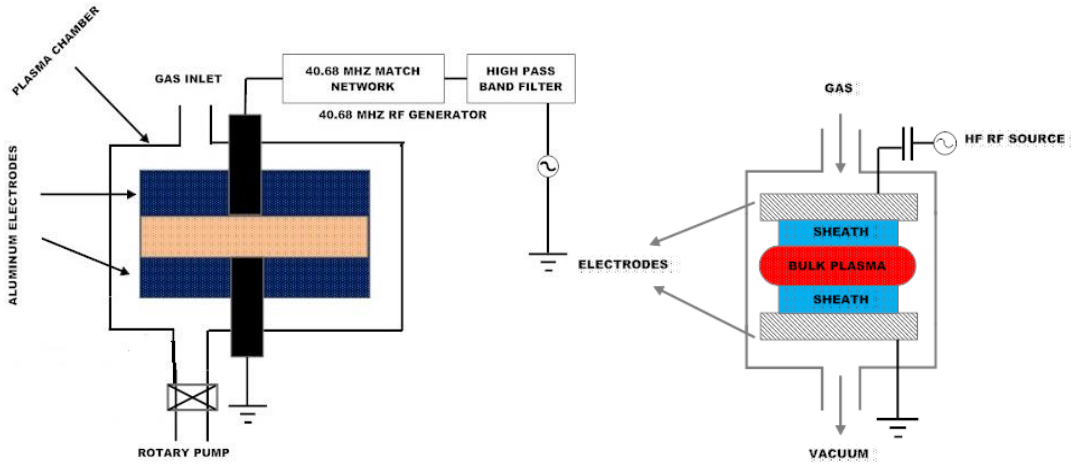

Figure 6.4: Schematic of single RF capacitively coupled plasma [38]

The distance of the probe to the upper and the lower electrodes were 1.5 and 2.5 cm, respectively. Thus, all diagnostic measurements were done in bulk plasma that is generated very close to the upper sheath region [38].

In our system, Pfeiffer Vacuum Single-Channel Measurement and Control Unit for Compact Gauges TPG 261 are used together for total pressure measurements. Our study is performed at 0.1-0.5 torr pressure.

Figure 6.5: Vacuum single-channel measurement and control unit [33]

6.1.1 Pump System

A vacuum is a volume of space that is empty of matter, but space can never be perfectly empty so the quality of a vacuum is indicated by the amount of matter remaining in the system. Generally, vacuum is measured by its absolute pressure.

Varian DS302 pump which is dual-stage, rotary vane pumps oil sealed, driven by a single-phase electric motor is used in our system. This pump system is suitable for pumping non-corrosive gases like nitrogen as used in our system. The pump works with force-feed lubrication, provided by an auxiliary gear-pump driven by the rotor of the vacuum pump itself [34] (see Figure 6.6).

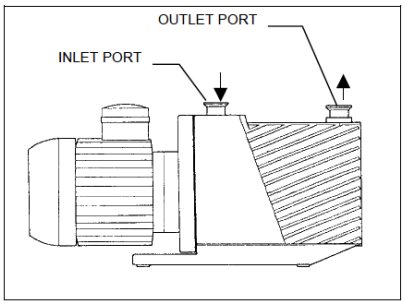

Figure 6.6: Schematic of the pump system [34]

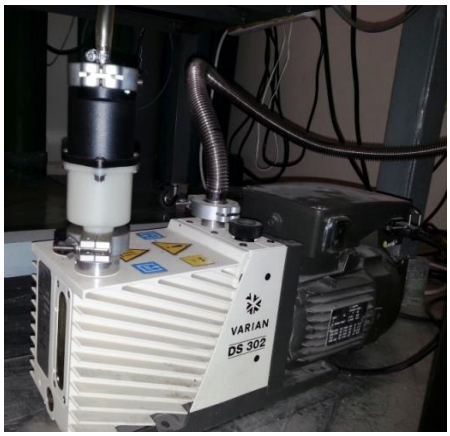

Figure 6.7: Photograph of the pump system

6.1.2 Plasma Power System

SEREN Industrial Power Systems, R601 Radio Frequency Power Supply is used to generate plasma in our system. The basic configuration shown below consists of the MC2 Controller, an AT-Series matching network, an RF Power source (generator), and a load/processing system. In this configuration, the MC2 and matching network operate independently from the RF power source and load/processing system.

The plasma impedance is automatically transformed from a mismatched condition to 50 Ohms regardless of load variations by the function of the AT-6 Automatic Matching Network using passive components with high voltage and current ratings, configured in a basic type "L" configuration.

The DC Voltage probe signal is connected to the MC2 Controller by the AT-Series Control Cable. The MC2 Controller can route the DC Voltage probe signal to the RF Generator for DC Voltage Control operation, to the user's system for monitoring, and display the DC Voltage on its front panel.

RF Input Power is 600 Watts Nominal, application dependent and the frequency is 40.68 Mhz [35]. Basic plasma processing system is given in Figure 6.8.

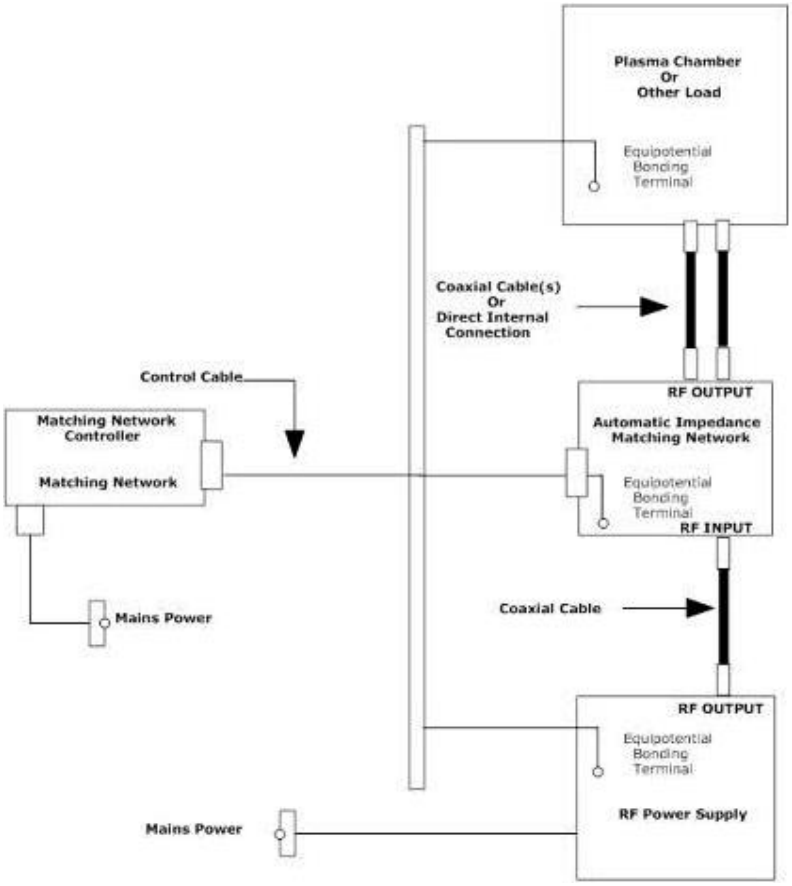

Figure 6.8: Basic Plasma Processing System [35]

6.2 ALP, Automated Langmuir Probe System

In order to assess the reliability of the manufactured probe for plasma measurements, a standard commercial probe is also used for plasma measurements in the same set up. Impedance Langmuir Probe and ALP system Control Unit are set in the plasma chamber. The probe is DC and RF compensated. Tip length of the probe is 5 mm and the probe radius is 0.195 mm. A typical system layout for the probe is shown below in Figure 6.9.

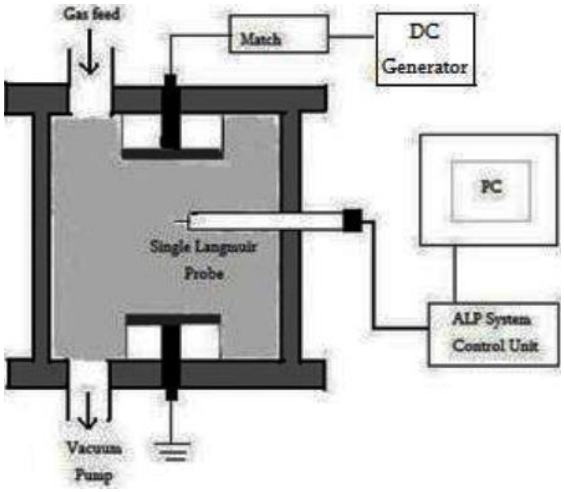

Figure 6.9: The ALP System™ Langmuir probe and vacuum system layout [25]

The ALP System controller supplies a connection between probes and software program. The probes are connected to rear panel of the controller with BNC cables and the controller is connected to the PC with an USB cable. The ALP System™ Langmuir Probe consists of a probe tip mounted in a push-fit cradle, a ceramic-coated probe shaft, integrated re-entrant ceramic feed through, flange, and filter/termination enclosure. The standard probe is shown in the following figure (Figure 6.10).

Figure 6.10: ALP System Langmuir probe

The Impedans ALP System™ electronics autonomously performs the data acquisition, control and initial analysis of the Langmuir Probe before passing the data to the ALP System™ software for analysis, display and data management [25]. ALP System Control Unit is given as in Figure 6.11.

Figure 6.11: ALP System Control Unit

In a RF discharge the plasma potential is vary with time, and, plasma-probe sheath shifts occur and distort the probe I-V characteristics [41]. In order to eliminate the RF noise signals (fluctuations and shifts) and to get better experimental calculations, compensation circuits are used [38]. ALP has such a compensation circuit which increases the probe-to-ground impedance to minimize the RF voltage drop across the probe sheath, and an extra 'compensation electrode' is added to reduce the probe sheath impedance [25]. In ALP, the RF compensation circuit, which is an RF band stop filter and thus includes inductors "*RF chokes - L1 and L2*" and capacitors "*C*", are connected to the probe close to the tip as shown in Figure 6.12. These chokes which have self-resonant frequencies at the plasma driving frequency are placed to increase the probe-to-ground impedance to minimize the RF voltage drop across the probe sheath [38].

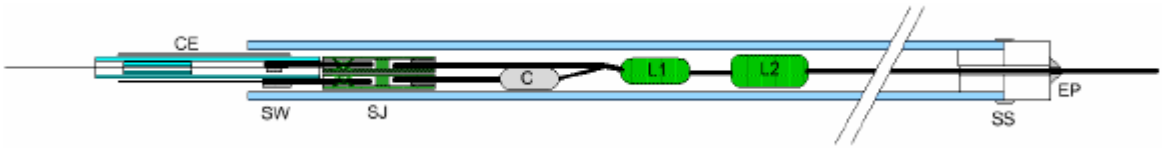

Figure: 6.12 Schematic diagram of an RF-compensated single Langmuir probe [20]

CHAPTER 7

MEASUREMENT RESULTS AND DISCUSSIONS

Although constructing and implementing a single Langmuir probe to obtain I-V characteristics is relatively a simple task, collecting exact data and analyzing them to extract accurate plasma parameters is quite difficult. Because of this difficulty in the Langmuir probe data interpretation, literature on this probe theory is extensive and new articles are published regularly as new approaches emerge [16]. As mentioned in Chapter 3, the theories that are commonly used to interpret the data give widely varying results, especially in the weakly ionized plasmas. One reason for this is that there is still no mature theory that treats the case accurately enough when there is only a few collisions between ions and neutral atoms in the plasma [41]. Two fundamental approaches which are called "thin sheath" and "thick sheath (OML regime)" analyses are introduced in this thesis. Additionally, Allen-Boyd-Reynolds (ABR) theory and Bernstein-Rabinowitz-Laframboise (BRL) are also used to analyze I-V characteristics in plasma measurements [22]. Allen-Boyd-Reynolds (ABR) theory is the first theory which suggests a thin sheath around a probe in 1957. Studies in the literature show that the calculations of plasma parameters can differ from each other when different probe designs and analysis methods applied [41].

7.1 Current-Voltage Characteristics

In our experiments, the probe voltage is biased by sweeping it from -10 V to +10 V by the Source Meter and the current data is collected from the same device to obtain I-V curve. We repeated the sweeps for the plasma generated under different pressures in order to determine the plasma potential, electron temperature and electron density. I-V curves taken from the designed probe for the different pressures are shown in Figure 7.1.

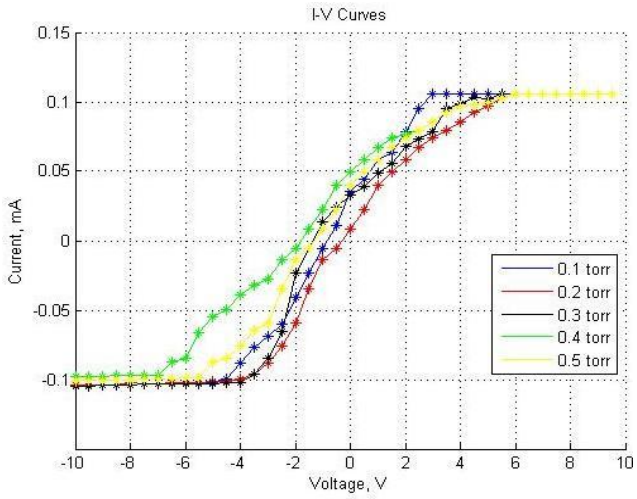

Figure 7.1: The *I-V* curves of the designed probe for different pressures

As mentioned before, the Automated Langmuir Probe (ALP) was also used to obtain I-V curve. One example of the data taken from the ALP System Langmuir probe is given in Figure 7.2.

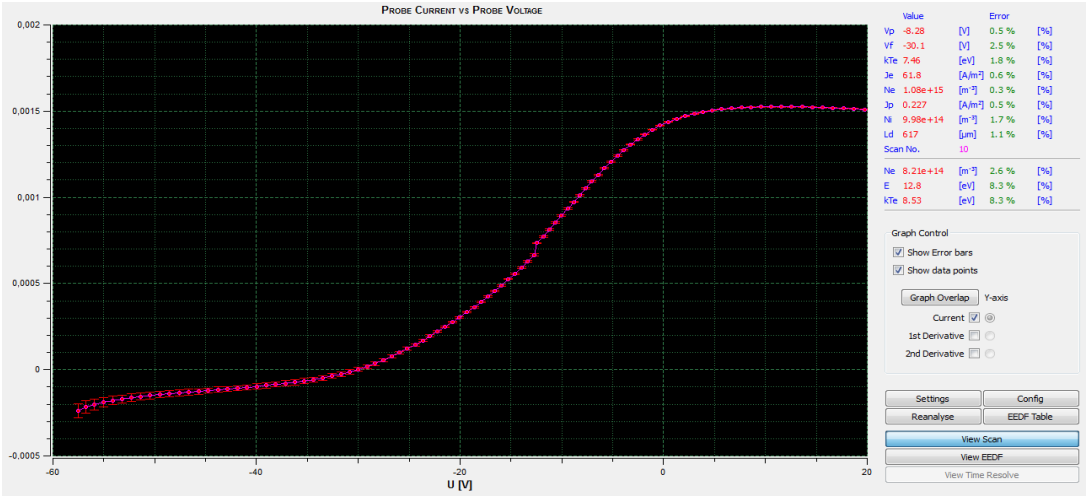

Figure 7.2: A data example of ALP System Langmuir Probe plasma measurements

Taking into account the previously recorded parameters for the plasma generated in the experimental setup at METU lab, we re-calculated the probe radius to Debye length ratio as follows:

Range of plasma temperature observed in this system is KT_e=10-30 eV and range of electron density that is typically observed in this system is $ne = 10^{14} – 10^{15}$ m^{-3}.

Therefore Debye length ranges from 0.743 mm to 4.06 mm and ratio of the probe radius to Debye Length then varies from 0.046 to 0.25, which implies that our probe operates under "thick sheath (OML)" regime. Therefore we will apply the OML approach in our calculations in this section. However, note that two different theories (which are "Lafromboise Orbital Motion" and "Allen, Boyd and Reynolds" theories) are automatically used for different plasma conditions in ALP probe system. Selection of the correct theory is based on the number of ion neutral collisions in the sheath [25].

7.1.1 Plasma Potential

As explained in Chapter 3, plasma potential is calculated from the maximum of the first derivative of I-V curve. Measurements for the normalized plasma potential under the pressure ranging from 0.1 Torr to 0.5 Torr are plotted in different colors in Figure 7.3.

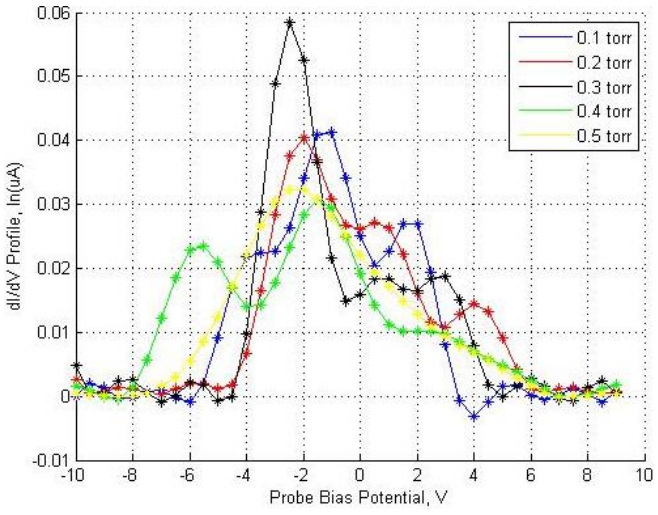

Figure 7.3: Normalised dI/dV Profile for V_p at maximum

In order to evaluate the accuracy of the designed probe, the V_p results are compared for two probes in 0.1-0.5 Torr pressures and measurement results are shown for Designed and ALP Probes in Figure 7.4.

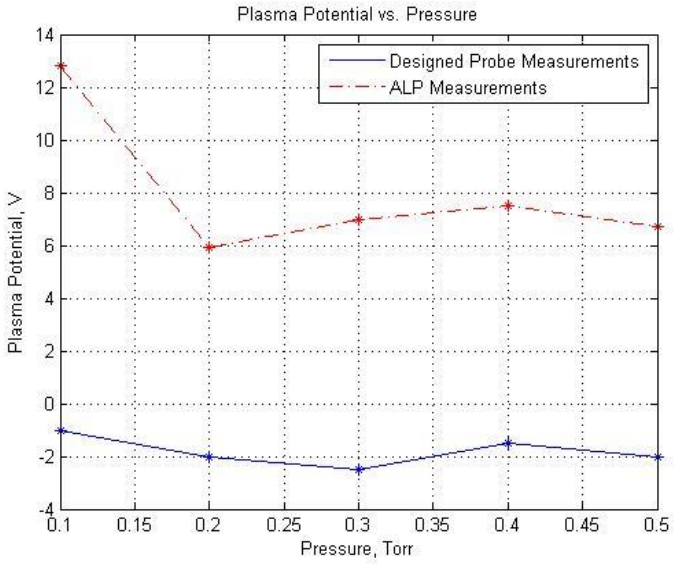

Figure 7.4: Plasma potential results of designed and ALP probes

Figure 7.4 shows that although the plasma potentials obtained from the Designed Probe are smaller than that of the results obtained from the ALP, the trend observed in plasma potential, V_p, for increasing pressure is similar. This result suggests that either our probe or the automated probe introduces a bias in the plasma potential measurements.

According to earlier studies of RF plasmas, capacitive coupling across space charge sheaths induces RF fluctuations in the plasma potential with respect to a laboratory 'ground potential'. Therefore in general measured plasma potential exhibits a fluctuation in the form of $\emptyset_p \sim \emptyset_{p0} coswt$, possibly accompanied by higher harmonics, where $\emptyset_p$ is an "unknown plasma potential" and w is the RF frequency [45]. In our measurements, the Langmuir Probe is operated with potentials that are set relative to vacuum chamber ground. Therefore, first, the effect of this biasing on the probe measurement must be considered. In the electron retardation region of a current-

voltage characteristic for a single probe, the fundamental component of plasma potential is given by

$$I = eA_{probe}\left[-\frac{n_{0}v_{e,th}}{4}exp\left(\frac{e(V-\emptyset_{p0}coswt)}{kT_e}\right)+n_s u_B\right], \quad (7.1)$$

where n_0 is the density of the "undisturbed" plasma, $v_{e,th}$is thermal velocity, n_s is density at the ion sheath edge, u_B is the speed of sound (Bohm speed) [45].

Eqn. (7.1) shows that there is now a non-linear RF component of current to the probe and it is difficult to measure. An example of the effect of an RF fluctuation of plasma potential on the current-voltage characteristic of a Langmuir probe is given in Figure 7.5 [45].

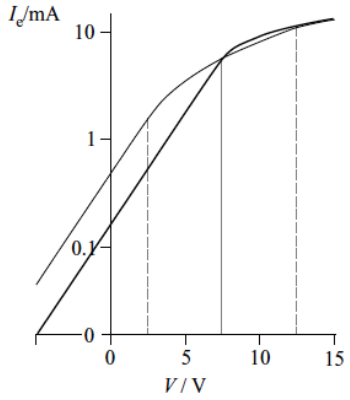

Figure 7.5: The effect of an RF fluctuation of plasma potential on the current-voltage characteristic of a Langmuir probe in a low-pressure hydrogen plasma with $n = 3.6x10^{15}m^{-3}$ [45]. The grey curve is the average current when $V_p = V_1 \cos wt$, the black curve is the "true" current.

Figure 7.5 shows that there is a shift in the electron retardation section of the curve to the left. This shift results in a plasma potential measurement smaller than the "true" value. In other words, the deficiency seen in our measurements with respect to the measurements from the automated probe in Figure 7.4 may be due to the lack of RF compensation in our probe design.

According to observations in RF plasmas, there may be shifts and perturbations in both floating potential and the local plasma potential measurements. Because RF plasma is very susceptible to probe perturbation, the greater absolute voltage shifts may result from even small fractional changes in the plasma potential. In order to compensate plasma potential, probe measurements can be made with respect to another probe or a strong RF compensation circuit which is specifically designed for the plasma of interest can be utilized, as explained in Chapter 6 [42].

7.1.2 Electron Temperature

As mentioned in chapter 3, electron temperature is obtained from the slope of the logarithm of the electron current in the transition region [22]:

$$KT_e = (\frac{dln\, I_e}{dV})^{-1}. \quad (3.16)$$

Electron temperatures are found for 0.1-0.5 Torr, and the graph obtained for each pressure is plotted separately below.

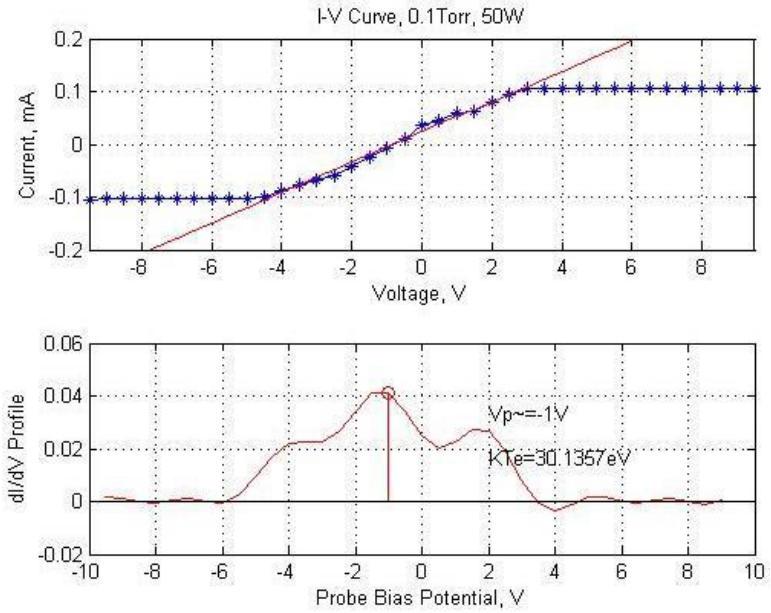

Figure 7.6: KT_e measurements result of Designed LP for 0.1 Torr, 50W

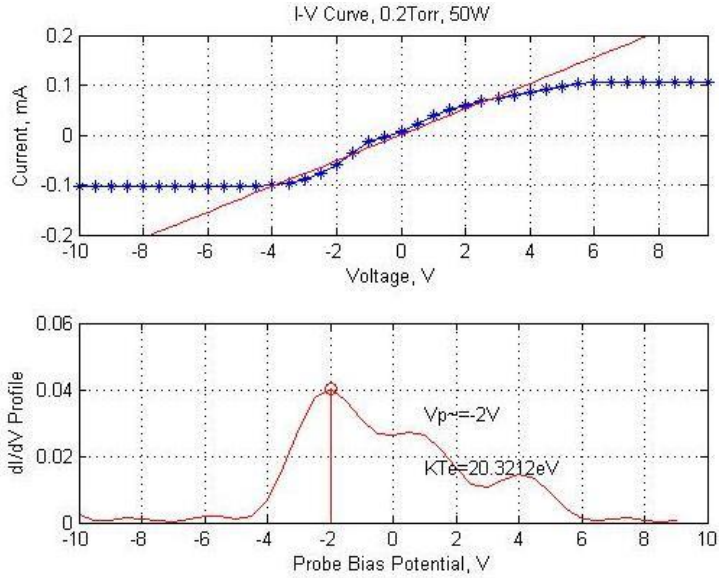

Figure 7.7: KT_e measurements result of Designed LP for 0.2 Torr, 50W

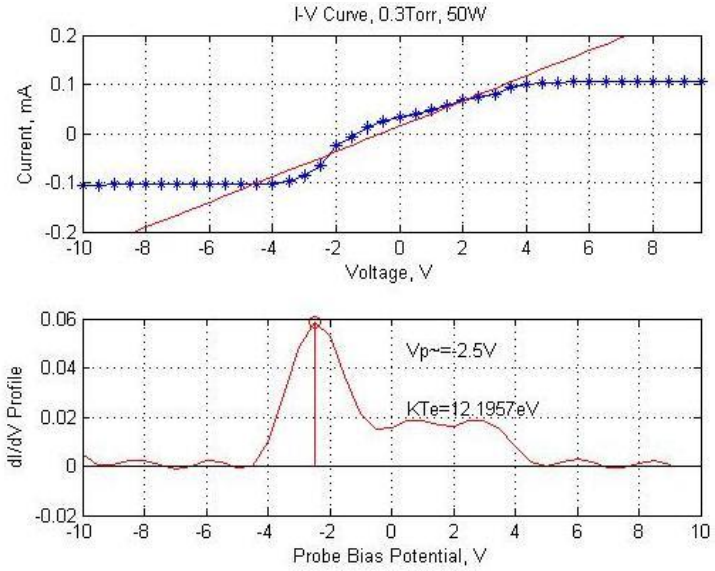

Figure 7.8: KT_e measurements result of Designed LP for 0.3 Torr, 50W

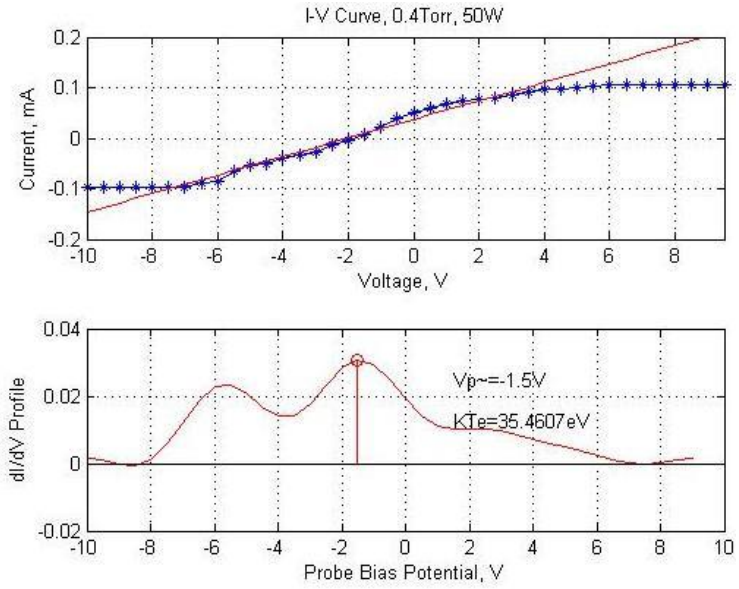

Figure 7.9: KT_e measurements result of Designed LP for 0.4 Torr, 50W

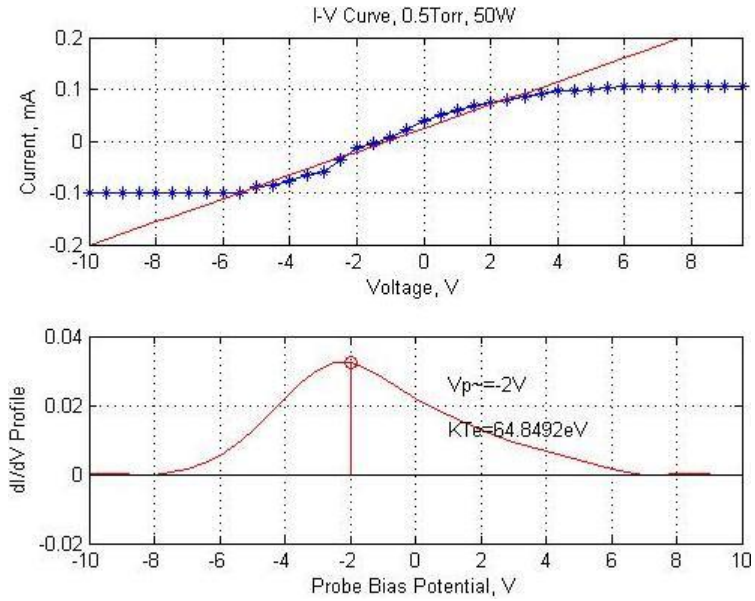

Figure 7.10: KT_e measurements result of Designed LP for 0.5 Torr, 50W

Figure 7.11 shows the comparison of electron temperature measurements obtained from both the designed probe and ALP in different colors.

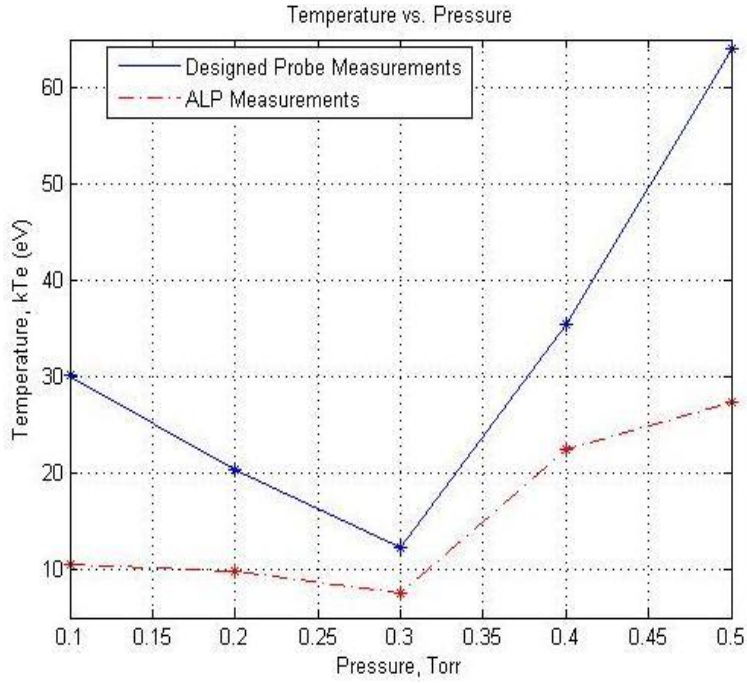

Figure 7.11: Electron temperature, KT_e values for Designed LP and ALP in 0.1-0.5 Torr

As seen in Figure 7.11, the similar electron temperature trend is observed in both probe results: the electron temperature makes a dip at 0.3 Torr. This dip results from the "α" and "Ɣ" modes in plasma.

Two distinct stable regimes named "α" and "Ɣ" modes were first observed by Lewitskii and according to Godyak and Kanneh, when fast electrons is produced in the sheath and they penetrates into the plasma zone then a critical concentration of additional charge is generated and this causes a transition in high pressures [37].

At low pressures "p<0.3 Torr", electrons are in low energy in the bulk plasma for achieving the potential barrier to pass through the sheath region but at sufficiently high pressures for "p>0.3 Torr", the electrons in the bulk plasma gains more energy and they move toward to the sheath region. Because of this movement, electron current in the bulk plasma decreases and the temperature of electrons increase [38].

Moreover, when we examine the electron temperature results of the designed handmade probe, the values of electron temperatures are seen bigger according to

ALP values and theoretical knowledge. Studies show that because the RF distorting voltage is normally quite high, the averaging of electron current extends into both the electron saturation current and ion saturation current regions. Therefore, the net result of KT_e is overestimated as the averaging of electron current is a much more complicated function and cannot be compensated with the simple approach we used in our probe design [42].

In summary, due to the fluctuations in RF plasma, electron temperature generally exceeds the true value and leads to a spuriously high apparent KT_e [39, 42]. With RF compensation circuit, this problem can be avoided.

7.1.3 Electron Density

To find the electron density, the equation (3.20) as given in Chapter 3, is used (OML region):

$$n_e = \frac{I_{sat}}{A_{probe}\sqrt{\frac{e(V_{s1}-V)}{m_i}}}\frac{\pi}{\sqrt{2}}. \qquad (3.20)$$

As mentioned in Chapter 3, the electron density is calculated using the OML assumption. In OML regime, the slope of I^2 versus V plot is proportional to n_e^2 [22]. The formula does not depend on KT_e, so n_e can be determined by fitting a straight line to the slope of an I^2-V plot [39]. In our calculations,

we used the following constants: m_i for nitrogen= $2.32\text{x}10^{-26}$kg, e is electron charge, e=$1.602\text{x}10^{-19}$c, A_{probe}=$1.32\text{x}10^{-5}$.

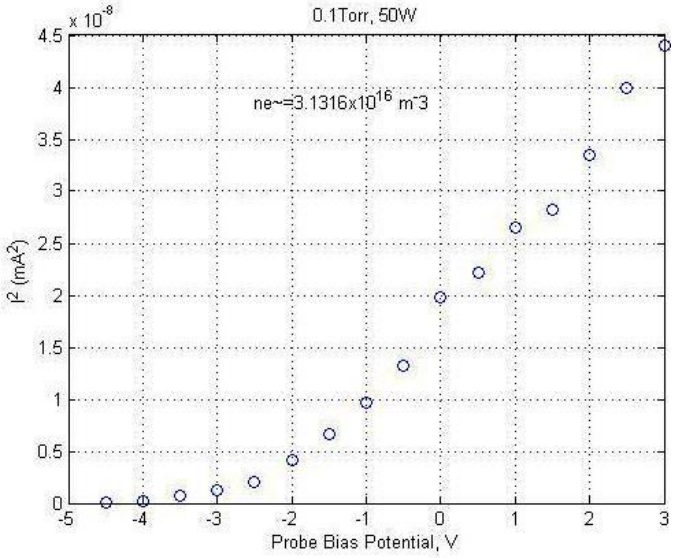

Figure 7.12: Electron density result from I^2-V graph for 0.1 Torr-50 W

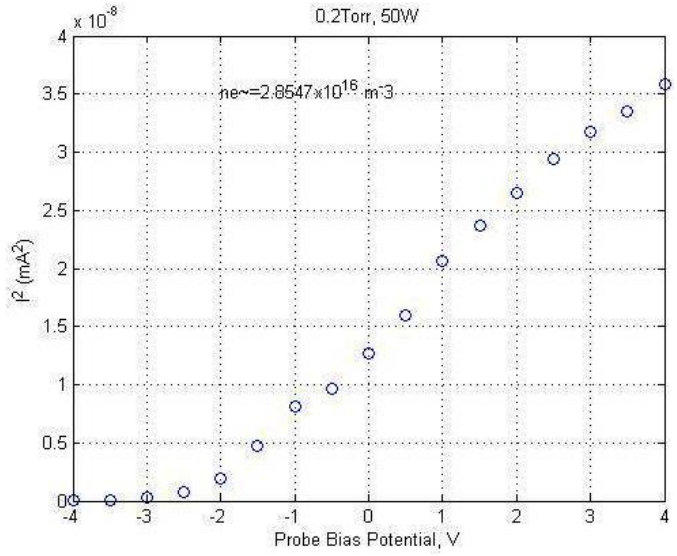

Figure 7.13: Electron density result from I^2-V graph for 0.2 Torr-50 W

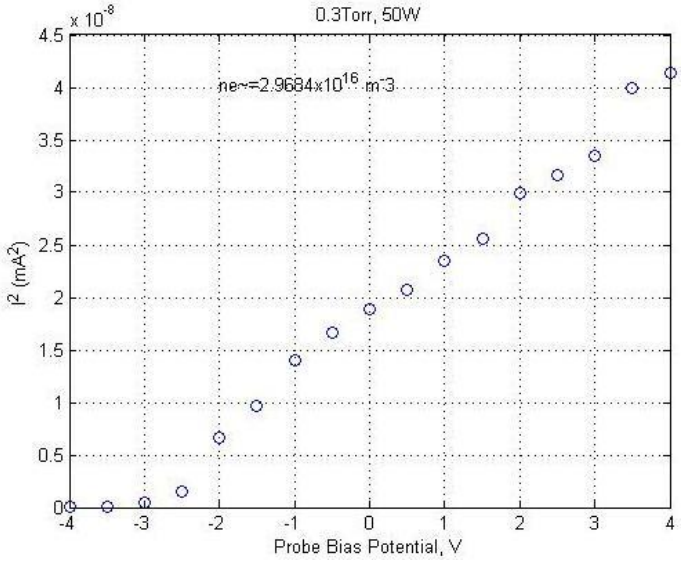

Figure 7.14: Electron density result from I^2-V graph for 0.3 Torr-50 W

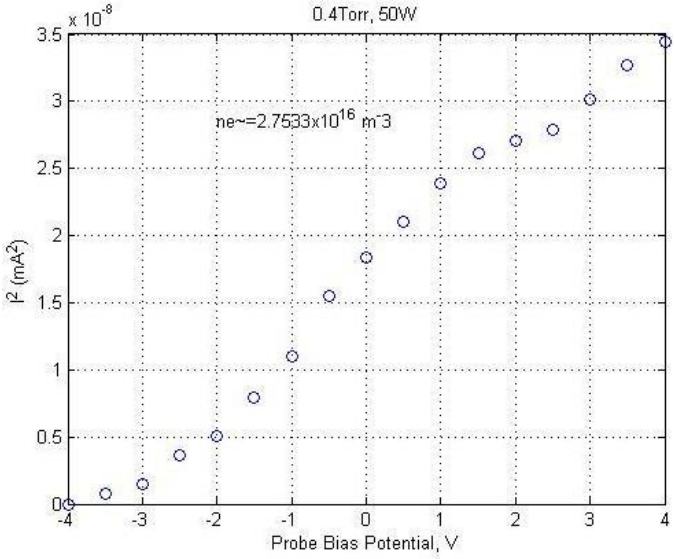

Figure 7.15: Electron density result from I^2-V graph for 0.4 Torr-50 W

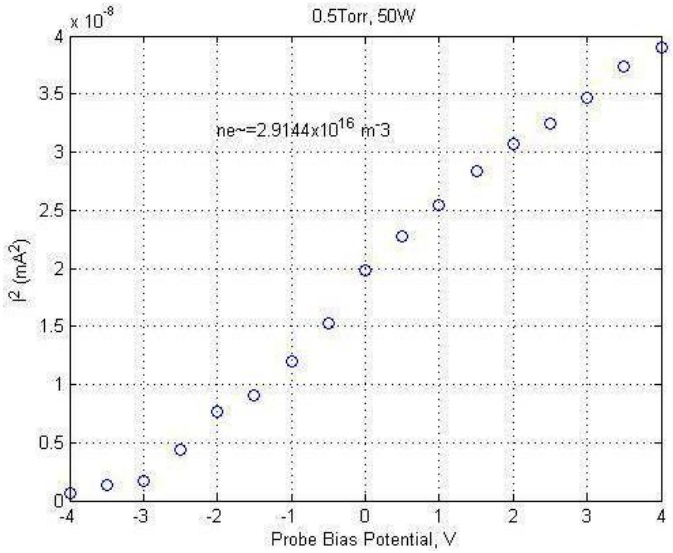

Figure 7.16: Electron density result from I^2-V graph for 0.5 Torr-50 W

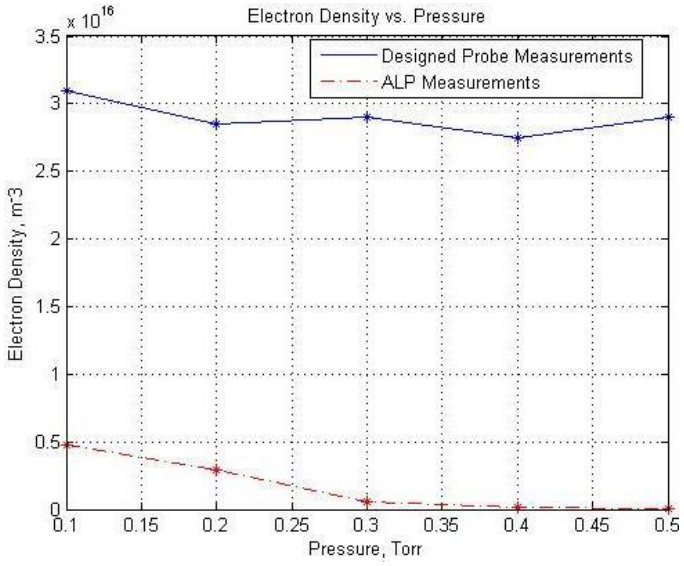

Figure 7.17: Electron density vs pressure graph for Designed LP and ALP probes

The results show that electron density decreases as pressure increases as expected because electrons gain more energy with pressure and pass the ambipolar barrier and escape to sheath region, decreasing the observed current [38]. Even though, this

decrease is more apparent in the ALP measurements, it is not seen as significantly in the measurements of the designed probe in Figure 7.17.

Comparison of the electron density results from the designed and ALP probes in Figure 7.17 shows another ambiguity: electron density measurements of the designed probe are bigger than that of the ALP probe. One reason for this difference may be due to the theories used for calculation of electron density in the designed probe and ALP system, as mentioned before, different theories commonly give different results due to presence of charge exchange ions [41]. Even the ion-neutral collisions are infrequent; ignoring these collisions in OML theory may cause the differences seen in the results. In the literature, different approaches are used to calculate the plasma density and it is showed that plasma densities calculated from the OML theory are often large in weakly ionized plasmas [46]. In another study, the current-voltage data is analyzed with Langmuir's Orbital Motion Limited theory, the Allen-Boyd-Reynolds (ABR) theory and the Bernstein-Rabinowitz-Laframboise (BRL) theory and the results show that ABR underestimates, BRL overestimates the density and OML theory gives better result of plasma density comparing to both two theories [41].

CHAPTER 8

CONCLUSION AND FUTURE WORK

In this work, a Single Langmuir probe design is given to be used for plasma measurements in low pressure plasma measurements, which consists of a 0.375 mm diameter and 11 mm length tungsten wire. The rest of the probe is coated by 4 ceramic tubes with different sizes whose total length of 32.5 cm. The basic working principle of Single Langmuir probes along with the criteria and measurement methodology applied in the design of the probe is also described. In addition, the technique that will be used in the analysis of the current-voltage characteristics to determine the local plasma potential, electron number density and temperature is discussed in detail. Then, the produced probe was used and tested for plasma measurements in low pressure vacuum chamber. The measurement results of the plasma potential, electron temperature and electron density and the comparisons of these results with that of Standard ALP System Langmuir Probe are presented and discussed in detail.

First of all, we successfully performed the experiments and took the measurements using our probe and probe circuit. Results from our probe show a typical I-V curve characteristic. Plasma potential, electron temperature and electron density that are obtained from this curve by applying the OML theory are in the same ball park of the measurements recorded in the literature for the low pressure RF plasmas. However, comparison of the plasma potential measurements from our designed probe with that from the ALP probe system in the same plasma setup showed that our probe's measurements are shifted to left in the plot, implying more negative plasma potential for the same plasma. This ambiguity may be the result of the fluctuations observed in RF plasmas, which typically cause shifts in the plasma potential measurements. In the literature, an RF compensation circuit is commonly used to mitigate the effects of RF signal effects in the measurements. Results may be improved by adding similar

RF compensation components to the probe circuit; however, this task is out of the scope of this work as the probe is designed to be used in DC plasma measurements in HET experiments.

Comparison of electron temperature results of the designed probe with the ALP results showed that our probe overestimates the electron temperature. The results also seem to exhibit greater values than that of the theoretical expectations. Similar to plasma potential values, the differences observed in the electron temperate are predicted to be due to RF fluctuations and resulting distorted plasma and floating potential. Thus, RF compensation circuit may be needed to obtain more accurate results [22].

The calculations to determine plasma density are made using "thick sheath (OML) analysis" for designed handmade probe. Comparison of the electron density results of the designed and ALP probes showed that the results of the designed probe are greater (about one order of magnitude) than that of ALP probe. One reason for this difference may be due to the approaches that are used to calculate the density from the I-V curves. Note that for our probe, we apply OML approach however two different theories which are "Lafromboise Orbital Motion" and "Allen, Boyd and Reynolds" theories are used for different plasma calculations automatically in ALP probe system. Studies in the literature show that ABR underestimates the plasma density which suggests that our designed probe with OML theory gives the results closer to the "true" plasma density values.

These works will provide a foundation for studying the plume and performance characteristics of a Hall Effect thruster using a single cylindrical Langmuir probe in the future. In the Figure 8.1, angular profiles of typical electron temperature and electron number density in the plume of a SPT-100 Hall Effect Thruster are presented [5]. These profiles show that in the plume of a SPT 100 electron temperature ranges from 0.5 to 1.6 eV and electron number density ranges from 10^{16} to 10^{17} m^{-3}. In other words, the properties of the plume plasma for a SPT-100 Type Hall Effect Thruster is approximately in the same range with the plasma generated in

our measurement system. This allows us to utilize the probe designed in this paper for the study of the plume of Hall Effect Thrusters in the future.

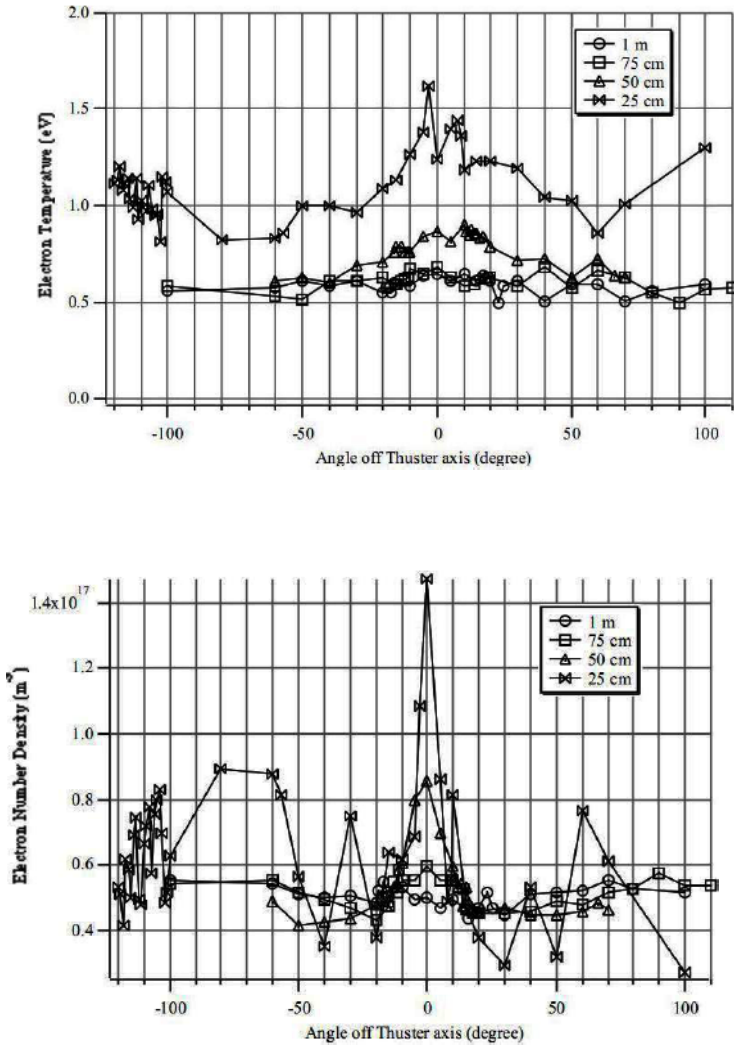

Figure 8.1: Angular profiles of electron temperature and electron number density from the SPT-100 exit plane [5]

In future work, RF compensation circuit can be made to obtain more accurate results. Also, the probe can be tested for analyzing plume of the Hall Effect Thruster in different regions.

REFERENCES

[1] D.M. Goebel and I. Katz, Fundamentals of Electric Propulsion: Ion and Hall Thrusters, Jet Propulsion Laboratory California Institute of Technology, March 2008.

[2] Ian J.E Jordan, Electric Propulsion: Which One for My Spacecraft, December 6, 2000.

[3] ESA Science & Technology: Electric Spacecraft Propulsion, Electric Versus Chemical Propulsion, July 24, 2014.

[4] Daniel Lucas Brown, Investigation of Low Discharge Voltage Hall Thruster Characteristics and Evaluation of Loss Mechanisms, The University of Michigan, p.6, 2009.

[5] Sang-Wook Kim, Experimental Investigations of Plasma Parameters and Species-Dependention Energy Distribution in the Plasma Exhaust Plume of a Hall Thruster, Aerospace Engineering in The University of Michigan, 1999.

[6] M. Martinez-Sanchez and J.E. Pollard, Spacecraft Electric Propulsion-An Overview, Journal of Propulsion and Power Vol.14, No.5, September-October 1998.

[7] Robert G. Jahn and Edgar Y. Choueiri, Electric Propulsion, Encyclopedia of Physical Science and Technology, Third Edition, Vol.5, 2002.

[8] Francis, F. Chen, Introduction to Plasma Physics and Controlled Fusion, Second Edition. Volume 1: Plasma Physics, Jan 31, 1984.

[9] Samuel T. Sawyer, Experimental Studies of Spacecraft Plasma Interactions: Facility Characterization and Initial Measurements, Virginia Polytechnic Institute and State University, June 9, 2009.

[10] The University of Michigan, Department of Aerospace Engineering, Plasmadynamics and & Electric Propulsion Laboratory, Plasma Diagnostics, Faraday Probe, July, 2014.

[11] Yassir Azziz S.B., Instrument Development and Plasma Measurements on a 200-Watt Hall Thruster Plume, Aeronautics and Astronautics in Massachusetts Institute of Technology, 2001.

[12] Fort Collins, "Plasma Controls, Faraday Probe", Colorado, LLC 2007-2012, http://www.plasmacontrols.com/products/Faraday.php, last visit: August 2014.

[13] A. Marek1, M. Jílek1, I. Picková1, P. Kudrna1, M. Tichý1, Emissive probe diagnostic in low temperature plasma – effect of the space charge and variations of the electron saturation current, Charles University in Prague, 28th ICPIG, Prague, Czech Republic, July 15-20, 2007.

[14] The University of Michigan, Department of Aerospace Engineering, Plasmadynamics and & Electric Propulsion Laboratory, Plasma Diagnostics, Emissive Probe, July, 2014.

[15] The University of Michigan, Department of Aerospace Engineering, Plasmadynamics and & Electric Propulsion Laboratory, Plasma Diagnostics, Retarding Potential Analyzer (RPA), July, 2014.

[16] Robert L. Merlino, Understanding Langmuir Probe Current-Voltage Characteristics, Department of Physics and Astronomy The University of Iowa, Iowa City, July 2007.

[17] Daniel Andrew Herman, The Use of Electrostatic Probes to Characterize the Discharge Plasma Structure and Identify Discharge Cathode Erosion Mechanisms in Ring-Cusp Ion Thrusters, Aerospace Engineering in Michigan University, 2005.

[18] Langmuir's Probe, http://www.physics.csbsju.edu/370/langmuir_probe.pdf, last visit: July 2014.

[19] K Dannenmayer, P Kudrna, M Tichy and S Mazouffre, Measurement of Plasma Parameters in the Far-Field Plume of a Hall Effect Thruste; Institue de Combustion, Aerothermique, Reactivite et Environnement, CNRS, Orleans, France, 2011.

[20] Francis, F, Chen, Langmuir Probes in RF Plasma: Surprising Validity of OML Theory, Plasma Sources Sci. Technol. Received 22 September 2008, in final form 7 April 2009, published 29 May 2009.

[21] Martin Lampe, Trapped Ion Effect on Shielding, Current Flow and Charging, of a Small Object in a Plasma; Washington, January 2003.

[22] Francis F. Chen, Langmuir Prob Diagnostics, Electrical Engineering Department University of California, Los Angeles, June, 2003.

[23] M. Touzeau, M. Prioul, S. Roche, N. Gascon, C. Perot, F. Darnon, S.BECHU, C.Philippe Kadlec, L.Magne, P.Lasgorceix, D.Pagnon, A.Bouchoule and M.Dudeck, "Plasma Diagnostic Systems for Hall-Effect Plasma Thrusters", Plasma Phys, Control Fusion, Printed in the UK, June 2000.

[24] M. A. Lieberman, A. J. Lichtenberg, Principles of Plasma Discharges and Materials Processing, U.S, 1994.

[25] Impedans System Made to Measure, ALP System Langmuir Probe, Installation and User Guide, Ireland, Revision: 2.10, May 2011.

[26] Loretta L. Jones, Chemistry Explained, Foundations and Applications, Ceramics, http://www.chemistryexplained.com/Bo-Ce/Ceramics.html, last visit: July 2014.

[27] A&N Corporation, High Vacuum Components Since 1965, ISO (QF/LF, KF, NW/ISO-K) Flanges Fittings, Retrieved July 2014.

[28] Kurt J. Lesker, Company, Flanges and Components, Technical Notes, KF (QF) Flanges,
http://www.lesker.com/newweb/flanges/flanges_technicalnotes_kf_1.cfm?pgid=0,
last visit: August 2014.

[29] Kurt J. Lesker, Company, Feedthroughs & Viewports, Electrical Feedthroughs, Instrumentational Feedthroughs, BNC Feedthroughs, KF Flange, Single-Ended, http://www.lesker.com/newweb/feedthroughs/instrument_feedthroughs_bnc_singleend.cfm?pgid=kf , Retrieved 2014.

[30] LewVac Components Ltd, Quality Components For Vacuum Technology, Vacuum Wires, Cables & Accessories, Push-on Connectors, FHP-BECU-2.4-CON.

[31] Thorlabs, Torr Seal Vacuum Epoxy, TS-10 Specification Sheet, May 5, 2014.

[32] Murat Çelik, Oleg Batishchev, Use of Emission Spectroscopy for Real-Time Assessment of Relative Wall Erosion Rate of BHT-200 Hall Thruster for Various Regimes of Opertaion, Aeronautics and Astronautics in Massachusetts Institute of Technology. Department of 2010.

[33] Operating Instructions Incl. Declaration of Conformity BG 805 195 BE/A (0110) 1, Single Gauge, Single-Channel Measurement and Control Unit for Compact Gauges, TPG 261, Pheiffer Vacuum, Deutschland.

[34] Varian Vacuum Technologies, Dual Stage Rotary Vane Pumps Instructions Manual, 87-900-937-01(D), Italy, October 2002.

[35] SEREN Industrial Power Systems Inc, RX01/LX01 Series Radio Frequency Power Supply Operator's Manual, Revision:1.09, Standard Configuration Document Number 6100220000, New Jersey, U.S.A.

[36] E.Y. Choueiri, Plasma Oscillations in Hall Thrusters, Electric Propulsion and Plasma Dynamics Laboratory, Princeton University, Princeton, 2000.

[37] V. Lisovskiy, Modes and the Alpha-Gamma Transition in RF Capacitive Discharges in N_2O at different RF Frequencisies, Laboratoire de Physique et Technologie des Plasmas, Ecole Polytechnique, Palaiseau 91128, France and Kharkov National University, Kharkov 61077, Ukraine, 2006.

[38] Ümmügül Erözbek-Güngör, Surface Modification of Unsized Pan-Based Carbon Fiber By Using High Frequency Single and Dual RF Discharge System, Physics Dept, Metu, February 2014.

[39] Francis F Chen, Langmuir Probe Measurements in the Intense RF Field of a Helicon Discharge, Electrical Engineering Department, University of California, Los Angeles, USA, September 2012.

[40] David Sirajuddin, Determination of Plasma Parameters of a Neon DC Plasma Using a Langmuir Probe, Langmuir Probe Lab Report, Nuclear Engineering & Radiological Sciences, February 2007.

[41] Francis F Chen, John D Evans and Wade Zawalski, Calibration of Langmuir Probes Against Microwaves and Plasma Oscillation Probes, Electrical Engineering Department, University of California, Los Angeles, USA, August 2012.

[42] John V. Scanlan, Langmuir Probe Measurements in 13.56 MHz Discharges, Dublin City University, September 1991.

[43] P M Bryant, Theory of Clindrical Langmuir Probes in Weakly Ionized, Non-Thermal, Stationary and Moderately Collisional Plasmas, Department of Electrical Engineering and Electronics, University of Liverpool, UK, November 2008.

[44] Demiral Akbar, The Non-Uniform Argon DC Glow Discharge System Parameters Measured With Fast Three Couples of Double Probe, Physics Dept, Metu, March 2006.

[45] Pascal Chabert and Nicholas Braithwaite, Physics of Radio-Frequency Plasmas, printed in the United Kingdom at the University Press, Cambridge, 2011.

[46] Z. Sternovsky, S. Robertson, and M. Lampe, The Contribution of Charge Ex-change Ions to Langmuir Probe Current. Department of Physics, University of Colo-rado, Boulder, CO 80309-0390 and Plasma Physics Division, Naval Research Labor-atory, Washington D.C., 20375-5346.

[47] J. E. Allen, Probe Theory-The Orbital Motion Approach, Department of Engineering Science, University of Oxford, UK, December 1991.

[48] Francis F. Chen, Langmuir Probe Analysis For High Density Plasmas, Electrical Engineering Department, University of California, Los Angeles, June 2000.

APPENDIX

Derivation of Ion Saturation Current Formulas

Let us consider when the potential of the probe is positive with respect to the plasma, electrons are attracted to it. The electrons move in a central field of force when the length of the probe is larger than its radius and energy and angular momentum are simultaneously conserved. In collision theory, with a target placed on the axis, 'impact parameter' is introduced as the perpendicular distance of the initial path from the axis. Electrons with large impact parameters can deflect passing orbits but electrons with low impact parameters collide with the probe. It is aimed to obtain an expression for the current collected by the probe. The trajectory of an electron on a path grazes the probe surface with an impact parameter *h* [45]. Figure A.1 shows the graphical display of an electron moving towards the probe where *h* is impact parameter, *p* is the distance of closest approach and r_p is the probe radius.

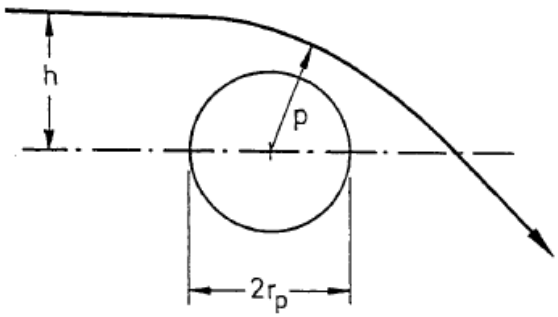

Figure A.1 shows the graphical display of an electron moving towards the probe [47]

J. E. Allen gives the derivation of the current collected by the probe for cylindrical geometry as the following equations [47].

Conservation of energy gives,

$$\frac{1}{2}m_e v^2 = \frac{1}{2}m_e v_p^2 - eV, \qquad \text{(A.1)}$$

where v_p is the velocity at the probe surface, V is the probe potential.

Conservation of angular momentum gives for an electron at grazing incidence,

$$m_e v h_p = m_e r_p v_p. \qquad \text{(A.2)}$$

Thus,

$$h_p = r_p(1 + V/V_0)^{1/2}, \qquad \text{(A.3)}$$

where the initial energy of the electron is eV_0, h_p is the effective radius of the probe.

Electrons with a narrow velocity range is also contributes to the current, that is given as,

$$dI = 2\pi r_p l e(1 + V/V_0)^{1/2}\,(v/\pi)dn, \qquad \text{(A.4)}$$

where the quantity $(v/\pi)d_n$ shows the flux crossing unit area considering electrons move in planes perpendicular to the axis.

Considering a Maxwellian distribution of velocities, the two dimensional version of the distribution gives

$$d_n = n_e\left(\frac{m_e}{2\pi KT_e}\right)e^{-m_e v^2/2KT_e} e 2\pi v dv, \qquad \text{(A.5)}$$

so that

$$dI = \frac{2n_e r_p l m_e e}{KT_e} v^2 e^{-m_e v^2/2KT_e}(1 + V/V_0)^{1/2} dv, \qquad \text{(A.6)}$$

which can be written as

$$dI = 4n_e r_p l e\left(\frac{2KT_e}{m_e}\right)^{1/2} x e^{-x^2}(x^2 + a^2)^{1/2} dx, \qquad \text{(A.7)}$$

where $x^2 = m_e v^2/2KT_e$ and $a^2 = eV/KT_e$.

By integration, the total current is obtained as,

$$I = 4n_e r_p le \left(\frac{2KT_e}{m_e}\right)^{1/2} \int_0^{\infty} xe^{-x^2}(x^2 + a^2)^{1/2}\, dx. \qquad \text{(A.8)}$$

For determination of the integral $\int_0^{\infty} xe^{-x^2}(x^2 + a^2)^{1/2}\, dx$, let $x^2 + a^2 = u^2$, then $2xdx = 2udu$.

$$\int_a^{\infty} u\, e^{-u^2+a^2} du = \left[-\frac{1}{2} ue^{-u^2+a^2}\right]_a^{\infty} + \frac{1}{2}\int_a^{\infty} e^{-u^2+a^2} du$$

$$= \frac{a}{2} + \frac{\sqrt{\pi}}{4} erfc(a) e^{a^2}$$

$$= \frac{\sqrt{\pi}}{4}\left[\frac{2a}{4} + e^{a^2} erfc(a)\right]. \qquad \text{(A.9)}$$

So the integral in (A.8) is evaluated as,

$$\int f(x)dx = \frac{\sqrt{\pi}}{4}\left(\frac{2\aleph}{\pi} + e^{\aleph} erfc\sqrt{\aleph}\right), \qquad \text{(A.10)}$$

where $\aleph = eV_p/KT_e$.

Then, the final expression of the current is now shown as,

$$I = 2\pi n_e r_p le \left(\frac{KT_e}{2\pi m_e}\right)^{1/2} \left(\frac{2\sqrt{\aleph}}{\sqrt{\pi}} + e^{\aleph} erfc\sqrt{\aleph}\right). \qquad \text{(A.11)}$$

Figure A.2 shows a plot of $\left[\left(2\sqrt{\aleph}/\sqrt{\pi}\right) + e^{\aleph} erfc\sqrt{\aleph}\right]$and a plot of $2(1 + \aleph)^{1/2}/\sqrt{\pi}$.

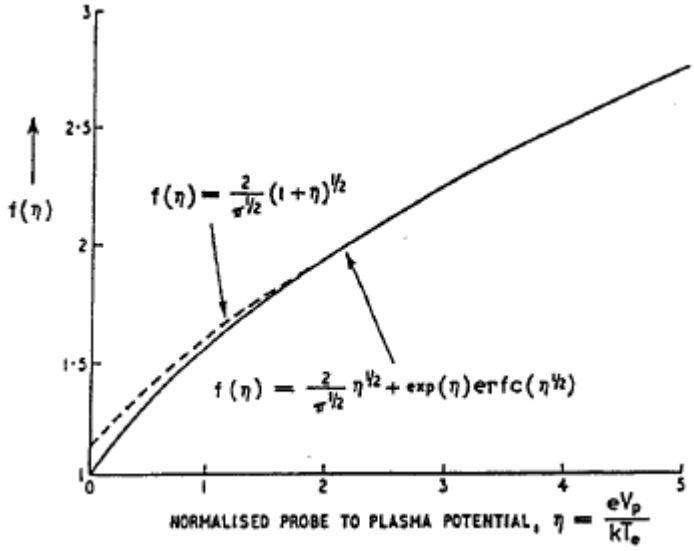

Figure A.2: A plot of the functional form of eqn. (A.11) together with a plot of the function $2(1+\aleph)^{1/2}/\sqrt{\pi}$.

Figure A.2 shows that the curves are indistinguishable for values of ℵ greater than 2. Thus, the final form of the current is given as,

$$I = 2\pi n_e r_p l e \left(\frac{KT_e}{2\pi m_e}\right)^{1/2} \frac{2}{\sqrt{\pi}} \left(1 + \frac{eV}{KT_e}\right)^{1/2}, \qquad \text{(A.12)}$$

when $eV_p/KT_e \geq 2$.

Therefore, a plot of I^2 versus V should be a straight line and from the slope of the curve, we get n_e.

It is seen that the corresponding equation for positive ion collection is given in eqn. (A.13) for cylindrical geometry.

$$I = 2\pi n_e r_p l e \left(\frac{KT_i}{2\pi m_i}\right)^{1/2} \frac{2}{\sqrt{\pi}} \left(1 - \frac{eV}{KT_i}\right)^{1/2}. \qquad \text{(A.13)}$$

It is seen that as $T_i \to 0, T_i$dependence is cancelled and a finite limiting value of the OML current is given in eqn. (A.14) [48].

$$I \xrightarrow[T_i \to 0]{} A_{probe} n_e \frac{\sqrt{2}}{\pi} \sqrt{\left(\frac{|eV|}{m_i}\right)} \qquad \text{(A.14)}$$

If we consider thin sheath, ions enter the sheath with Bohm velocity where $u_B = (KT_e/m_i)^{1/2}$,

so that the saturation ion current is given as,

$$I_{sat} \approx \alpha n_e A_{probe} u_B. \qquad \text{(A.15)}$$

Eqn A.15 shows that I_{sat} is independent of V because the effect of sheath is very little to the probe radius, r_p. Here, α is the ion density at the sheath edge, with $\alpha \approx 0.5$. Conditions in the pre sheath determines the exact value of α.